

The Performance of Combined Solar Chimney System for Power Generation and Seawater Desalination

Mohamed Fateh Yosif

Submitted to the
Institute of Graduate Studies and Research
in partial fulfilment of the requirements for the Degree of

Master of Science
in
Mechanical Engineering

Eastern Mediterranean University
December 2014
Gazimağusa, North Cyprus

Approval of the Institute of Graduate Studies and Research

Prof. Dr. Elvan Yılmaz
Director

I certify that this thesis satisfies the requirements as a thesis for the degree of Master of Science in Mechanical Engineering.

Prof. Dr. Uğur Atikol
Chair, Department of Mechanical Engineering

We certify that we have read this thesis and that in our opinion it is fully adequate in scope and quality as a thesis for the degree of Master of Science in Mechanical Engineering.

Prof. Dr. Hikmet Ş. Aybar
Supervisor

Examining Committee

1. Prof. Dr. Hikmet Ş. Aybar

2. Prof. Dr. Fuat Egelioglu

3. Asst. Prof. Dr. Tahir Abdul Hussain

ABSTRACT

Energy and fresh water shortages are two important problems which the whole world faces. Making use of solar energy to desalt seawater or brackish water and setting up solar chimney power systems can go some way to solve the aforementioned problems. In this study an alternative method of heat and moisture extraction from seawater under the collector of a solar chimney system for power generation and seawater desalination with a high-efficiency condenser (HEC) is investigated with the objective of estimating its performance.

In seawater desalination one-dimensional compressible flow model was employed. The combined solar chimney system for power generation and seawater desalination (CSCSPD) can achieve simultaneously multitargeted production such as power and freshwater. The performance of CSCSPD is studied and investigated mathematically and economically.

The mathematical investigation is done by using some parameters from the pilot setup in Dalian, China. the mathematical modeling was constructed by employing the matrix laboratory software (MATLAB) to achieve accurate estimations for variations in the parameters. The aim of the mathematical modeling is to investigate and obtain the optimal working of the power plant .

The investigation that relates to the economic value of the project is estimated by employing a methodological approach based on revenue analysis. In this regard, the revenue analysis is based on the price of fresh water and electric power in Dalian,

China. Furthermore, the economic model is developed by utilising MATLAB software.

The final results obtained indicated that the price of the water from the integrated power plant compares favourably to the price range of fresh water produced by conventional energy supply and wind energy supply. It can be concluded that the application of the multi-product system will enhance the economic performance of a solo solar chimney system (SSCS).

The results of the proposed mathematical and economic model clearly show how parameters of the CSCSPD affects ascending or descending to enhance the efficiency of integrated power plant performance.

The integrated system would significantly improve the utilization efficiency of solar energy.

Keywords: CSCSPD, MATLAB software, Integrated system, Solar power plant, Total electric power, Efficiency of power plant, mass flow rate, condenser.

ÖZ

Enerji ve tatlı su sıkıntısı bütün dünyanın karşı karşıya kaldığı iki önemli sorundur. Güneş enerjisinden yararlanılarak deniz suyu ve acı sudan tatlı su elde edilebilir ve güneş enerjisi baca sistemleri kurarak yukarıda sözü edilen sorunları çözmek için yol katedilebilir. Bu çalışmada alternatif bir yöntem olarak enerji üretimi ve deniz suyunu tuzdan arındırılması için deniz suyundan ısı ve nem çıkartılmasında yüksek verimli kondenseri olan bir güneş baca sisteminin performansı incelenmiştir.

Deniz suyunun tuzdan arındırılmasında tek boyutlu sıkıştırılabilir akış modeli kullanıldı. Elektrik üretimi ve deniz suyunu tuzdan arındırma için kombine güç ve desalinasyon güneş baca sistemi (KGDGBS) kullanılarak aynı anda güç ve tatlı su üretimi elde edilebilir. KGDGBS'nin performansı çalışıldı, matematiksel ve ekonomik olarak incelendi.

Matematiksel incelemede Dalian, Çin'deki pilot kurulumdan elde edilen parametreler kullanıldı. Matematiksel modellemede parametrelerdeki değişimlerden dolayı doğru tahminleri bulmak için matrix laboratory (MATLAB) yazılımı kullanıldı. Matematiksel modellemenin amacı güç santralının optimal çalışmasını incelemek ve elde etmektir.

Projenin ekonomik değeri ile ilgili inceleme gelir analizine dayalı bir metodolojik yaklaşım kullanılarak tahmin edildi. Bu bağlamda gelir analizi Dalian, Çin'deki tatlı su ve elektrik enerjisi fiyatlarını dayanmaktadır. Ayrıca, ekonomik modelleme MATLAB yazılımı kullanılarak geliştirilmiştir. Elde edilen nihai sonuçlara göre entegre santralden elde edilen tatlı su maliyetleri, geleneksel enerji ve rüzgar

enerjisinin kullanımı ile elde edilen tatlı su maliyet aralığı ile kıyaslandığında netice olumludur. Kombine sistemin uygulanması ile yalnız güneş baca sisteminin ekonomik performansının artıracığı sonucuna varılabilir.

Önerilen matematiksel ve ekonomik modellemede elde edilen sonuçlardan, KGDGBS'nin çalışma parametrelerinin entegre sistemin performansını nasıl artırıp azalttığını açıkça göstermektedir. Entegre sistem, önemli ölçüde güneş enerjisi kullanım verimliliğini artıracak.

Anahtar kelimeler: kombine güç ve desalinasyon güneş baca sistemi, MATLAB software, Entegre sistem, Güneş enerjisi santrali, Toplam elektrik, Güç santrali verimliliği, kütle akış hızı, kondenser.

DEDICATION

TO THE GREAT IRAQ

TO MY FAMILY

TO MY FRIENDS

ACKNOWLEDGMENT

Writing this thesis was quite a challenge. I worked hard to get to the point where I am now - writing my thank you's (yes, I have made it!) - But I definitely could not have gotten here without the support of many people. I would like to take the opportunity to thank some of you here. There is not enough space to thank everyone, so if I have not mentioned you, please do not think I forgot you!

I would like to thank my supervisor, Prof. Dr. Hikmet Ş. Aybar, for the patient guidance, encouragement and advice he has provided throughout my time as his student. I have been extremely lucky to have a supervisor who cared so much about my work, and who responded to my questions and queries so promptly.

I thank my parents, parents in law (Dr. Khalil and his wife Intisar) and my brothers' Omar and Mustafa, my brother in law Mohammed Khalil and his wife Rosul for always believing in me and for the warm memories; I have of my childhood years. I would like to take this opportunity to give a very special thank you to my father who was the light for my way and my mother for being such a warm and caring person, for always being there for me. You are my sun!

I thank with love to my wife. My dear wife has been my best friend and a great companion, loved, supported, encouraged, entertained, and helped me get through this agonizing period in the most positive way.

Finally, I would like to thank all my instructors, and research assistance of my department, who played a constructive role in my academics. They also made my life

as a member of the Mechanical Engineering Department family at Eastern Mediterranean University, a very interesting and memorable experience.

TABLE OF CONTENTS

ABSTRACT	iii
ÖZ	v
DEDICATION	vii
ACKNOWLEDGMENT	viii
LIST OF TABLES	xiii
LIST OF FIGURES	xiv
LIST OF ABBREVIATIONS	xviii
LIST OF SYMBOLS	xix
1 INTRODUCTION	1
1.1 Objective of Study	2
1.2 Thesis Organization	3
2 LITREATURE REVIEW	5
3 MATHTMATICAL MODEL.....	13
3.1 The Chimney	15
3.2 The High-Efficiency Condenser	21
4 PARAMETERS AND RESULTS	24
4.1 Variations with Collector Radius.....	26
4.2 Variations with Atmospheric Solar Radiation	27
4.3 Variations with MFR of Condensed Vapor at HEC	28
4.4 Variations with Chimney Height	29
4.5 Variations with Chimney Radius	31
4.6 Variations with Pressure Difference	32
4.7 Variations with Inlet Chimney Velocity	33

4.8 Variations with Effectiveness of Condenser.....	34
4.9 Variations with Mass Flow Rate of Ambient Air at Condenser Inlet.....	36
4.10 Variations with Condenser Radius	37
4.11 Variations of Mach number at Chimney Outlet	38
4.12 Variations with Total Latent Heat	39
4.13 Variations with Mass Flow Rate of Operating Air at Chimney Outlet	40
4.14 Variations with Maximum Difference in Temperature between Operating Air and Ambient Air at Condenser Inlets	42
4.15 Variations with Efficiency of Air Turbine Generator.....	43
4.16 Variations with Efficiency of Water Generator.....	44
4.17: Variations of CSCSPD efficiency with total electric power output from CSCSPD	45
5 ECONOMIC ANALYSIS.....	46
5.1 Economic Model.....	48
5.2 Variations with Collector Radius.....	50
5.3 Variations with Chimney Height	51
5.4 Variations with Service Life	52
5.5 Variations with Annual Interest Rate	53
5.6 Variations with MFR of condensed Vapor in the chimney and in HEC	54
5.7 Variations with Running Hours	55
6 CONCLUSION	58
6.1 Mathematical and Economic Conclusions.....	58
6.2 Ecological and Social Conclusions.....	59
6.3 Future Challenges	60
REFERENCES.....	62

APPENDICES	68
Appendix 1: The code of MATLAB for mathematical method	69
Appendix 2: The code of MATLAB for economic model	87

LIST OF TABLES

Table 4.1: The parameters and results for CSCSPD.....	25
Table 5.1: Comparison of economic performance of the CSCSPD system with different operation periods	56
Table 5.2: The unit price of freshwater that works with multiple sources energies [2].	57

LIST OF FIGURES

Figure 2.1: The solar updraft tower in Manzanares, Spain [8].....	6
Figure 2.2: Solar chimney power plant description [9].....	6
Figure 2.3: Schematic diagram of the integrated system [18].....	8
Figure 2.4: Conceptual diagram of a solar power-driven humidification dehumidification system for brackish desalination [23].....	11
Figure 2.5: Schematic diagram of experimental system for a solar power-driven Humidification-dehumidification system for brackish desalination [23].....	11
Figure 2.6: SSCS diagram [4].....	12
Figure 2.7: CSCSPD diagram [4].....	12
Figure 4.1: Variations of total electric power output from CSCSPD due to radius of solar collector.....	26
Figure 4.2: Variations of CSCSPD efficiency due to radius.of solar collector	27
Figure 4.3: Variations of total electric power produced from CSCSPD with atmospheric solar radiation	28
Figure 4.4: Variations of CSCSPD efficiency with atmospheric solar radiation.....	28
Figure 4.5: Variations of total electric output power from CSCSPD due to MFR of condenser condensed vapor.....	29
Figure 4.6: Variations of CSCSPD efficiency due to MFR of condenser condensed vapor.....	29
Figure 4.7: Variations of total electric power output from CSCSPD with chimney height.....	30
Figure 4 8: Variations of CSCSPD efficiency with chimney height	30

Figure 4.9: Variations of total electric power output from CSCSPD with chimney radius	31
Figure 4.10: Variations of CSCSPD efficiency with chimney radius.....	32
Figure 4.11: Variations of total electric power output from CSCSPD with pressure difference.....	33
Figure 4.12: Variations of CSCSPD efficiency with pressure difference.....	33
Figure 4.13: Variations of total electric power output from CSCSPD with inlet chimney velocity.	34
Figure 4.14: Variations of CSCSPD efficiency with inlet chimney velocity.	34
Figure 4.15: Variations of the MFR of condensed vapor in the HEC with its effectiveness.....	35
Figure 4.16: Variations of total electric power output from CSCSPD with effectiveness of the condenser.	35
Figure 4.17: Variations of CSCSPD efficiency with effectiveness of the condenser.....	36
Figure 4.18: Variations of total electric power output from CSCSPD with mass flow rate of ambient air at condenser inlet.	36
Figure 4.19: Variations of CSCSPD efficiency with mass flow rate of ambient air at condenser inlet.	37
Figure 4.20: Variations of total electric power output from CSCSPD with condenser radius.....	38
Figure 4.21: Variations of CSCSPD efficiency with condenser radius.	38
Figure 4.22: Variations of total electric power output from CSCSPD with Mach number at chimney outlet.....	39
Figure 4.23: Variations of CSCSPD efficiency with Mach number at chimney outlet	39

Figure 4.24: Variations of total electric power output from CSCSPD with total latent heat.	40
Figure 4.25: Variations of CSCSPD efficiency with total latent heat.....	40
Figure 4.26: Variations of total electric power output from CSCSPD with mass flow rate of operating air at chimney outlet.	41
Figure 4.27: Variations of CSCSPD efficiency with mass flow rate of operating air at chimney outlet.....	41
Figure 4.28: Variations of total electric power output from CSCSPD with maximum difference in temperature between operating air and ambient air at condenser inlets.	42
Figure 4.29: Variations of CSCSPD efficiency with maximum difference in temperature between operating air and ambient air at condenser inlets.	42
Figure 4.30: Variations of total electric power output from CSCSPD with efficiency of air turbine generator.....	43
Figure 4.31: Variations of CSCSPD efficiency with efficiency of air turbine generator.	43
Figure 4.32: Variations of total electric power output from CSCSPD with efficiency of water generator	44
Figure 4.33: Variations of CSCSPD efficiency with efficiency of water generator ..	44
Figure 4.34: Variations of CSCSPD efficiency with total electric power output from CSCSPD.....	45
Figure 5.1: Variations of annual revenue of electricity with collector radius.....	51
Figure 5.2: Variations of annual price of fresh water production with collector radius.	51
Figure 5.3: Variations of annual revenue of electricity with chimney height.....	52

Figure 5.4: Variations of annual price of fresh water production with chimney height.	52
Figure 5.5: Variations of annual average investment with service life.....	53
Figure 5. 6: Variations of annual price of fresh water production with service life. .	53
Figure 5.7: Variations of annual average investment with annual interest rate.	54
Figure 5.8: Variations of annual price of fresh water production with annual interest rate.....	54
Figure 5.9: Variations of annual price of fresh water production with MFR of vapor that condensed both in chimney and condenser	55

LIST OF ABBREVIATIONS

CSCSPD	Combined solar chimney system
CSCS	Classic solar chimney system
GHG	Greenhouse gas
HEC	High-efficiency condenser
HDH	Humidification dehumidification
LEC	Levelised electricity cost
MATLAB	Matrix Laboratory
MED	Multi effects desalination
MFR	Mass flow rate
NTU	Number of Transfer Units
PV	Photovoltaic panel
SCPS	Solar chimney power system
SCPP	Solar chimney power plant
SSCS	Solo solar chimney system

LIST OF SYMBOLS

A	Area (m^2)
A_{ch}	Area of the chimney (m^2)
A_{coll}	Area of the collector (m^2)
A_{cond}	Area of the condenser (m^2)
C	Speed of sound (m s^{-1})
CR_2	Capacity ratio of operating air at chimney outlet ($\text{kW/ }^\circ\text{C}$)
CR_{a_2}	Capacity ratio of ambient air at condenser inlet ($\text{kW/ }^\circ\text{C}$)
CR_{min}	Minimum capacity ratio of operating air ($\text{kW/ }^\circ\text{C}$)
C_p	Specific heat capacity ($\text{kJ kg}^{-1} \text{K}^{-1}$)
C_{p_2}	Specific heat capacity of operating air at chimney outlet ($\text{kJ kg}^{-1} \text{K}^{-1}$)
C_{p_a}	Specific heat capacity of ambient air at condenser inlet ($\text{kJ kg}^{-1} \text{K}^{-1}$)
D	Any diameter (m)
D_{ch}	Diameter of the chimney (m)
D_{coll}	Diameter of the collector (m)
D_{cond}	Diameter of the condenser (m)
DF	Density factor
ω	Moisture content of operating air ($\text{kg}_{\text{water}}/\text{kg}_{\text{dry air}}$)
ω_1	Moisture content of operating air at chimney inlet ($\text{kg}_{\text{water}}/\text{kg}_{\text{dry air}}$)
ω_2	Moisture content of operating air at chimney outlet ($\text{kg}_{\text{water}}/\text{kg}_{\text{dry air}}$)
ω_3	Moisture content of operating air at condenser outlet ($\text{kg}_{\text{water}}/\text{kg}_{\text{dry air}}$)
g	Gravitational acceleration (m.s^{-2})
z	Any height (m)
H_1	Chimney height (m)

h_{fg}	Latent heat from water (KJ Kg ⁻¹)
h	Specific enthalpy (J kg ⁻¹)
\dot{Q}_w	Required heat for evaporation (KJ s ⁻¹)
i	Annual interest rate (years)
k	Specific heat ratio, 1.4
L_{cond}	Latent heat of condensation (kJ kg ⁻¹)
$MACH_1$	Mach number of operating air at chimney inlet
$MACH_2$	Mach number of operating air at chimney outlet
\dot{m}	Mass flow rate (kg s ⁻¹)
\dot{m}_a	Mass flow rate of ambient air at condenser inlet (kg s ⁻¹)
\dot{m}_f	Mass flow rate of operating air (kg s ⁻¹)
\dot{m}_{f_1}	Mass flow rate of operating air at chimney inlet (kg s ⁻¹)
\dot{m}_{f_2}	Mass flow rate of operating air at chimney outlet (kg s ⁻¹)
\dot{m}_g	Mass flow rate of ambient air at sea level with ambient air temperature at chimney height (kg s ⁻¹)
n	Factor of pressure drop at the turbine: Service life of the integrated power plant system (years)
P	Static pressure (Pa)
P_0	Static pressure at 0 m above sea level (Pa)
P_1	Static pressure at chimney inlet (Pa)
P_2	Static pressure at chimney outlet (Pa)
P_3	Atmospheric pressure at condenser outlet (Pa)
P_v	Partial pressure of water vapor (Pa)
P_d	Partial pressure of dry air (Pa)
P_{sv}	Saturated vapor pressure (Pa)

P_{sv0}	Saturated vapor pressure at 0 °C (Pa)
\dot{W}_{at}	Electric power produced by the air turbine generator (W)
\dot{W}_{wg}	Electric power produced by water turbine generator (W)
\dot{W}_{total}	Total electric power produced from integrated power plant (W)
R	Specific gas constant ($J\ kg^{-1}\ K^{-1}$)
R_d	Specific gas constant of dry air ($J\ kg^{-1}\ K^{-1}$)
R_v	Specific gas constant of wet air ($J\ kg^{-1}\ K^{-1}$)
RH	Relative humidity (percentage)
r	Any radius (m)
I	Solar radiation ($W\ m^{-2}$)
T	Static temperature (°C)
T_1	Static temperature of operating air at chimney inlet (°C)
T_2	Static temperature of operating air at chimney outlet (°C)
T_3	Static temperature of operating air at condenser outlet (°C)
T_0	Stagnation temperature (°C)
T_{0_1}	Stagnation temperature of operating air at chimney inlet (°C)
T_{0_2}	Stagnation temperature of operating air at chimney outlet (°C)
T_{a_2}	Stagnation temperature of ambient air at condenser inlet (°C)
T_{a_3}	Stagnation temperature of ambient air at condenser outlet (°C)
u	Velocity in vertical direction ($m\ s^{-1}$)
u_1	Velocity of operating air at chimney inlet ($m\ s^{-1}$)
u_g	Velocity of ambient air at sea level with ambient air temperature at Chimney height ($m\ s^{-1}$)
β	Mean gradient of air density in the chimney ($kg\ m^{-3}$)
β_a	Mean gradient of ambient air ($kg\ m^{-3}$)

$\dot{m}_{\text{water}1}$	The MFR of chimney condensed vapor ($\text{kg} \cdot \text{s}^{-1}$)
$\dot{m}_{\text{water}2}$	The MFR of condenser condensed vapor ($\text{kg} \cdot \text{s}^{-1}$)
ΔP	The difference produced by pressure between the ambient air and the base of the chimney (Pa)
ΔQ	The latent heat released from vapor (W)
€_{at}	The price of air turbine generator (€)
$\frac{\text{€}_{coll}}{\text{m}^2}$	The price of solar collector for square meter in euro currency (€)
$\frac{\text{€}_{ch}}{\text{m}^2}$	The price of chimney for square meter in euro currency (€)
$\frac{\text{€}_{cond}}{\text{m}^2}$	The price of condenser for square meter in euro currency (€)
F_{pp}	The cost of the integrated power plant (€)
F_{yr}	The annual average investment (€)
\dot{W}_y	The annual power output (kWh)
E_{power}	Revenue received by the annual power output (€)
M_{water}	The annual freshwater productivity of the integrated system (ton)
M_{CO_2}	The amount of CO ₂ emission reduction (ton)
E_{CO_2}	Revenue received by carbon credits (€)
ρ_{water}	Density of water ($\text{kg} \cdot \text{m}^{-3}$)
$COST_{\text{water}}$	The annual price of fresh water productivity ($\text{€} \cdot \text{m}^{-3}$)
ξ	The annuity coefficient
ε	Condenser effectiveness
η	Efficiency
θ	Coefficient of total pressure loss
ρ_{a_0}	Density of ambient air at sea level ($\text{kg} \cdot \text{m}^{-3}$)
ρ_1	Density of operating air at chimney inlet ($\text{kg} \cdot \text{m}^{-3}$)

ρ_2	Density of operating air at chimney outlet (kg m^{-3})
ρ_{a_2}	Density of ambient air at condenser inlet (kg m^{-3})
ρ_v	Density of water vapor (kg m^{-3})
ρ_g	Density of ambient air at sea level with ambient air temperature at Chimney height (kg m^{-3})
η_{at}	The efficiency of air turbine generator
η_{wg}	The efficiency of water turbine generator
η_{pp}	The efficiency of integrated power plant

Chapter 1

INTRODUCTION

Energy and water are essential for life and coexistence between communities living on the planet and for survival in our modern world. In many areas of developed and developing societies, control and utilization of water and energy resources has driven economic evolution and progress. However, many parts of the world suffer from shortage of electric energy and fresh water supplies [1].

Depleting of fossil fuels and adverse effect of burning fossil fuels such as air pollution and greenhouse effect have increased the usage of renewable energy technologies.

Solar energy is environmentally more friendly, sustainable, pure, neat and useful for long term use. Eventually, it is now clearly one of the most favorable options to deal energy scarcity, weather fluctuation and energy saving.

Seawater desalination is one of the epidemic processes of obtaining considerable quantities of fresh water. Solar energy is used to desalt seawater or brackish water in solar chimney power systems can actually resolve the above-mentioned problems (i.e., energy and fresh water shortage) in some aspects [2].

The solar chimney principle was invented in 1978 by Professor J. Schlaich. The first system of solar chimney power plant (SCPP) was consists of: a collector, a thermal chimney, a turbine, and an energy storage layer [2].

A (SCPP) usually consists of a circular transparent canopy or a roof lifted to a certain altitude from the ground with a chimney or circular tower at its middle. The chimney houses one or more turbo-generators seated at its base. Radiation from the sun heats the collector roof and the ground surface below it. The heated floor in transition heats the adjacent air. The hot air underneath the collector flows towards and up into the central chimney to the turbo-generators [3]. A large number of pilot setups were constructed and tested in various parts of the world [4].

Wang et al. [5] suggested a new principle to produce electricity and freshwater from SCPS installed near the sea. The (CSCSPD) system was a combination of the following parts: 1- solar collector, 2-solar chimney, 3- air turbine, 4- high-efficiency condenser (HEC). This system is especially suitable for areas located near the sea or lakes [4].

1.1 Objective of Study

The study has two major purposes: the first aim is to design a HEC by using effectiveness–number of transfer units (NTU) method. The other aim is to develop an economic model to investigate the system's performance. The economic model was developed by employing MATLAB software. It is aimed to obtain accurate results and perform simulation to get optimum results.

Moreover, this study investigates the aggregate electric power delivered from the joined solar-based chimney incorporated with seawater desalination. It also examines the effectiveness of the consolidated plant that is affected by the thermal and physical impacts, such as specific humidity, relative humidity, density, specific heat capacity, temperature, stagnation temperature, latent heat of vapor, Mach number at the chimney

outlet, mass flow rate (MFR) of operating air at chimney outlet, the maximum temperature difference at HEC inlets, and MFR of ambient air at height of the chimney.

Other parameters investigated such as the difference in pressure, solar radiation, chimney inlet velocity, area of the chimney, area of the collector, cross sectional area of the HEC, effectiveness of HEC, efficiency of the air turbine, efficiency of the water generator, MFR of condensed vapor in the condenser, the height of the chimney.

The results can be accomplished by using the MATLAB software program based on an energy balance by mathematical modeling of compressible flow theory in the chimney (one -dimensional) and theoretical analysis as well.

Finally, the CSCSPD system is analyzed in terms of its economic benefits and its revenue collecting potential. In this regard its success can be measured from not only in industrial or agricultural terms, but how it benefits the community in general.

1.2 Thesis Organization

In chapter 2, information regarding the historical background of renewable energy is covered. It comprises seawater desalination, solar chimney power plants, working principles and components of solar chimney power plants including solar collectors, chimneys, turbine generators, and condensers. Moreover, an overview of the historical importance of some of these projects in renewable energy is examined with regard to their impact on their development within the scientific world as well as their effect in the world at large and how best they can be improved in the future.

In chapter 3, mathematical modeling using the energy balance equations is presented. This model works on theoretical assumptions and special one dimensional compressible flow theory in the chimney.

In chapter 4, important parameters (mentioned earlier), are varied and investigated in order to measure the effects of these parameters on the performance of CSCSPD. The results of the performance of the combined solar chimney power plant under existing parameters presented.

In chapter 5, an economic analysis was presented. Revenue analysis was employed to investigate the economic performance of the CSCSPD system.

Chapter 6 presents a comprehensive conclusion that covers all the aspects of thesis. These include an examination of the mathematical underpinnings of the approach, an economic and ecological analysis of the process as well as discussion of its social impact. However, in the interests of enhancing and improving the mathematical and economic models, some recommendations for future research are mentioned.

Chapter 2

LITREATURE REVIEW

A crisis in the ready availability of fresh water combined with a general energy crisis worldwide are the two most pressing problems that we face today. Using the solar energy to desalinate seawater and brackish water by constructing solar chimney power systems is one way to confront this [6].

Desalination systems driven by renewable energy have been widely debated as a new method to desalinate efficiently in an environmentally friendly manner. Delyannis et al. [1] has reviewed using solar energy as a source of renewable energy for desalination systems. Using solar energy in distillation dated back to medieval times. In recent times, some research has been conducted and some plants such as the Coober–Pedy distillation plant, The Abu–Dhabi multi effects desalination (MED) plant, the Las Salinas distillation plant and the Patmos distillation plant have been constructed. A solar dryer for salt recovery was designed and tested, using an MED plant that consists of solar collectors and a chimney. A draft of air is generated through the chimney that accelerates evaporation and helps in the operation of the desalination of water in the collector. This same concept that applies in the chimney is also used in SCPP.

In 1931, a German scientist, Hanns Gunther, was the first to describe in a publication the concept of the solar chimney to be used in SCPP.

In 1978, Professor J. Schlaich demonstrated the solar chimney power system [7]. In 1981, a pilot solar chimney power plant [8-10] was constructed in Manzanares, Spain (Figure 2.1 & Figure 2.2). It was also around this time that a number of pilot setups were built in different parts of the world and research continued in the field [4].

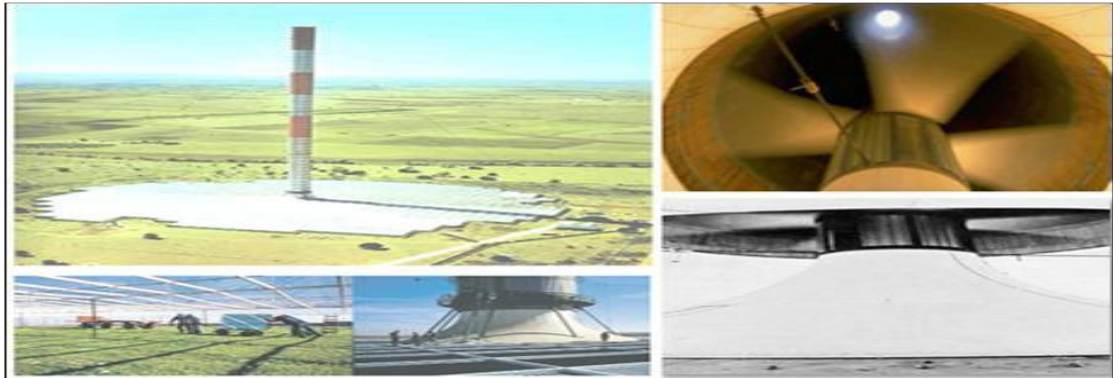


Figure 2.1: The solar updraft tower in Manzanares, Spain [9].

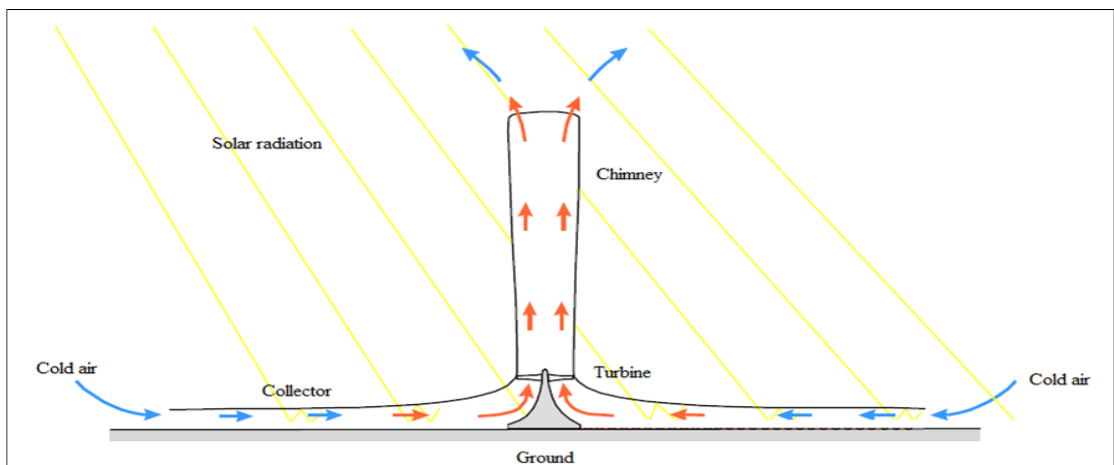


Figure 2.2: Solar chimney power plant description [10].

Following on from these early experiments, there was a growing interest in the scientific community in these type of projects and in particular about the great possibilities of SCPS and its application around the world [10-14].

From the thermodynamic point of view, researchers found that SCPS is significantly important for power plants working with solar energy; thus, it is subject to the laws of thermodynamics. The transformation efficiency factor of the SSCS does not reach $>1\%$, even in more appropriate circumstances [15], because the temperature of the heated air (heat origin) minimized by the collector is minimum.

Using theoretical analysis in [2], the SSCS value of utilization efficiency is around 0.74%.

Using solar energy in the distillation of fresh water from salty water is a process of thermal desalination that is called solar distillation. A solar still is a solar device aimed to seize the evaporated seawater by condensing it on a low temperature cover and distilling it, a solar still can be of various sizes.

In the solar still, the latent heat of the condensed water vapor is consumed directly to the cold air [16], and the vapor is condensed on a glass cover. The fresh water productivity is aligned in this process. If the latent heat utilized for the cold air was increased the higher the productivity would be. This also causes the increment in the temperature of seawater and further improvement in the production of freshwater. The control of heat loss help the system to control the condensation latent heat and when used again, it will improve either the solar energy utilization efficiency or the water productivity. Due to the large heat capacity, seawater is considered to be the storage for solar energy.

Very few research has been conducted that looks at those power plants that combine the production of both electrical power and freshwater. Whereas, various studies have

been done and research carried out on both systems individually. The main concept of using the SCPS is to produce electrical power and freshwater utilizing the same process and within the same time frame [5] see Fig 2.3.

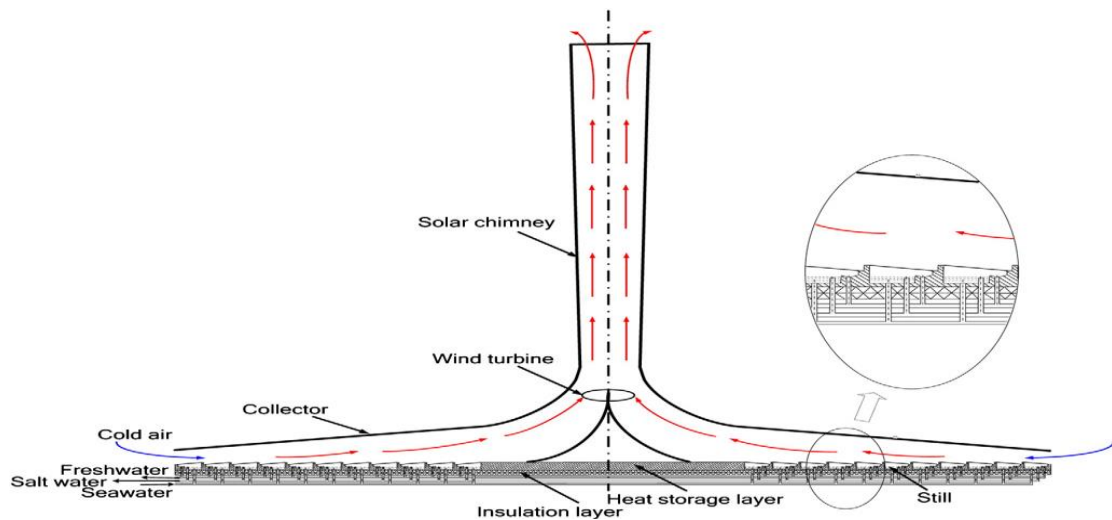


Figure 2.3: the solar still system' diagram [5].

Zuo et al. [2], investigated and developed individually two mathematical methods for a one-dimensional flow in the solar still desalination system and the SSCS. According to the theoretical analysis, the integrated system can dramatically improve the solar energy utilization efficiency as well as the efficiency of land resource utilization. In the meantime, the ecological, social and economic advantages can also be significant. The integrated system is ideal for development in Northwest China.

Zuo et al. [6], proposed a solar chimney integrated with seawater desalination as a prototype model for the experimental integrated system. Its performance and effectiveness was examined during real weather conditions. The experimental results refer to the simultaneous multi-targeted production that can be achieved, like fresh water and electricity power.

Zuo et al. [17], presented an unsteady-state mathematical model of the flow and heat transfer of the solar still desalination system under no-load conditions. The influence of heat collector structural parameters on the system has been studied and investigated. The results show that the draft force, airflow temperature, negative pressure and velocity rise of the integrated system increased dramatically with the increase in the collector diameter. The collector diameter has no effects on the glass cover temperature, seawater temperature and hourly freshwater yield per unit area. Due to the increase in the height of the collector inlet, the negative pressure and temperature rises, while the velocity, the temperature of the cover and the seawater temperature decreases. The amplitude value of the temperature of the cover drops more rapidly than the water temperature. The hourly freshwater yield decreases in certain periods and increases at other times. The influence of the collector inlet height on the characteristics of an integrated system has a slope to weaken with the height of the collector inlet increase.

Zou et al. [18], introduced an unsteady-state mathematical model of the heat transfer and flow of the solar still integrated system under no-load conditions. Here, features of the pressure distribution field, the temperature of the solar still integrated system and the velocity was studied. An optimization method based on the temperature distribution field in the region, with a set wind turbine was also examined. The results found that the relative pressure within the system has negative value. The temperature and relative pressure are higher, the temperature distribution is irregular and the stream is gradually getting slower at the base of the centre of solar collector. At the end of the collector and the entry of the solar chimney, the negative pressure amplitude reached its maximum point, therefore the wind turbine established at the place that considered as the ideal region. In order to optimize the geometric dimensions of the

negative pressure, the draft force, the passage of local flow and the velocity can be improved and the loss of energy can be decreased. The airflow flowing characteristics in the collector converted little after the optimization of the geometric dimensions; the optimization does not essentially effect the freshwater production in the still.

A humidification–dehumidification (HDH) process driven by a photovoltaic (PV) panel was examined by Wang et al. [19], in this process, the brackish water was desalinated under a free or forced convection mode. In this regard, a scale reactor implemented to refine sodium chloride (NaCl) -simulated brackish water. The main factors influencing the evaporation and condensation rates were calculated. The decreasing temperature of cooling water increased the rate of condensation of the water. The condensation and water evaporation mass flow rates increased with the increasing temperature of evaporative brackish water. The force convection mode brought about a higher freshwater yield than the free convection mode under given optimal conditions. With the forced convection, the highest freshwater yield was $0.873 \text{ kg}\cdot\text{m}^{-2}\cdot\text{d}^{-1}$ achieved at the evaporative temperature $T_0=64.3 \text{ }^\circ\text{C}$. A preparatory cost analysis displayed that the water produced (free convection) from the solar power-driven HDH desalination process had a cost comparable to the drinking water gained by traditional water treatment plants. This study showed that the HDH treatment was technically and economically functional for brackish water desalination (Figures 2.4 & 2.5).

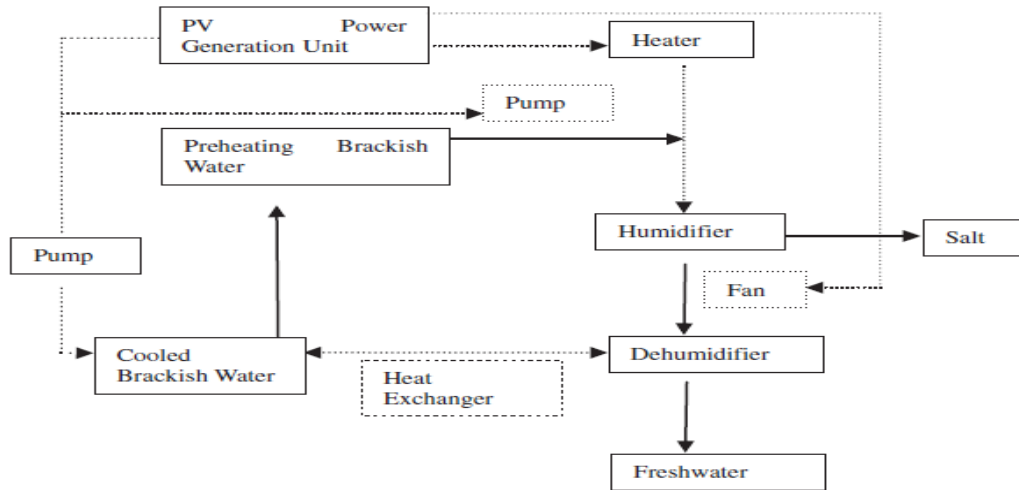


Figure 2.4: Conceptual diagram of a solar power-driven humidification-dehumidification system for brackish desalination [19].

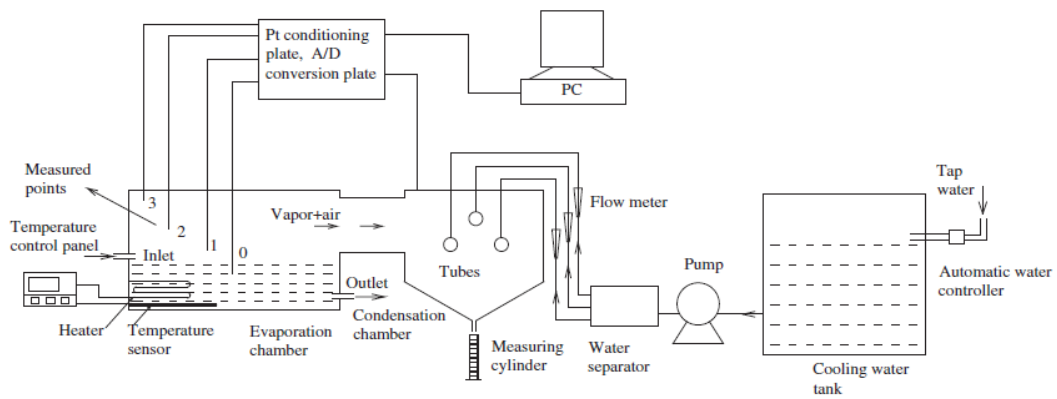


Figure 2.5: Schematic diagram of experimental systems for a solar power-driven Humidification-dehumidification system for brackish desalination [19].

In the system presented by Zhou et al. [4], seawater pumped from the sea opens to air in the collector, where warm and saturated operating air is driven out by solar energy. The air turbine installed on the chimney bottom leads by the saturated operating air to produce electric power. In this process, the warm air contains vapor inside and the chimney condenses it into fresh water using a HEC placed at the top of the chimney and fresh water holding large gravitational potential energy utilized for power generation through water turbine generators is installed at ground level. To complete the theoretical analysis, a mathematical model of energy balance has been applied to

demonstrate the performance of Wang's concept, and a comparison between revenue analysis results with those of SSCS by Zhou et al. [4] see Fig 2.6 and Fig 2.7.

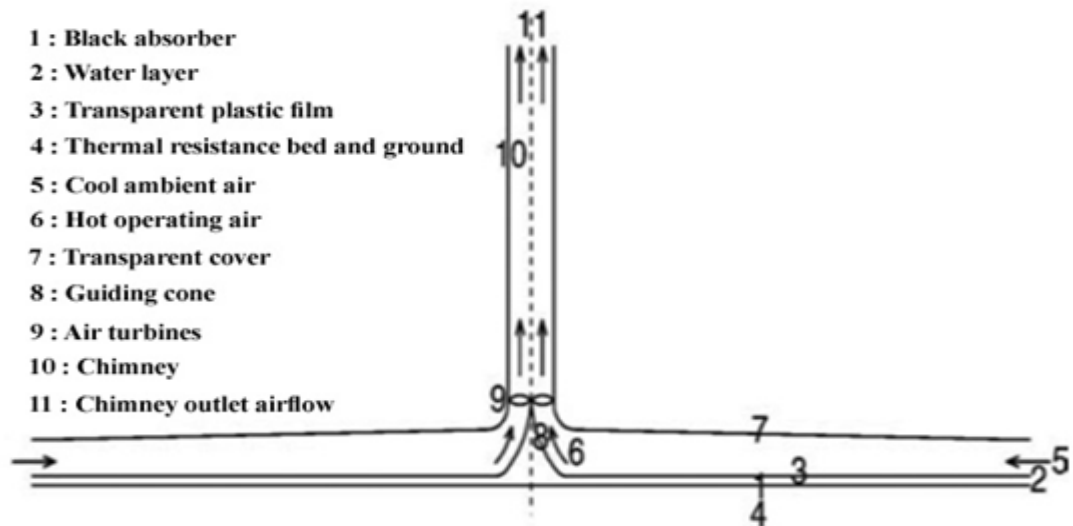


Figure 2.6: SSCS diagram [4].

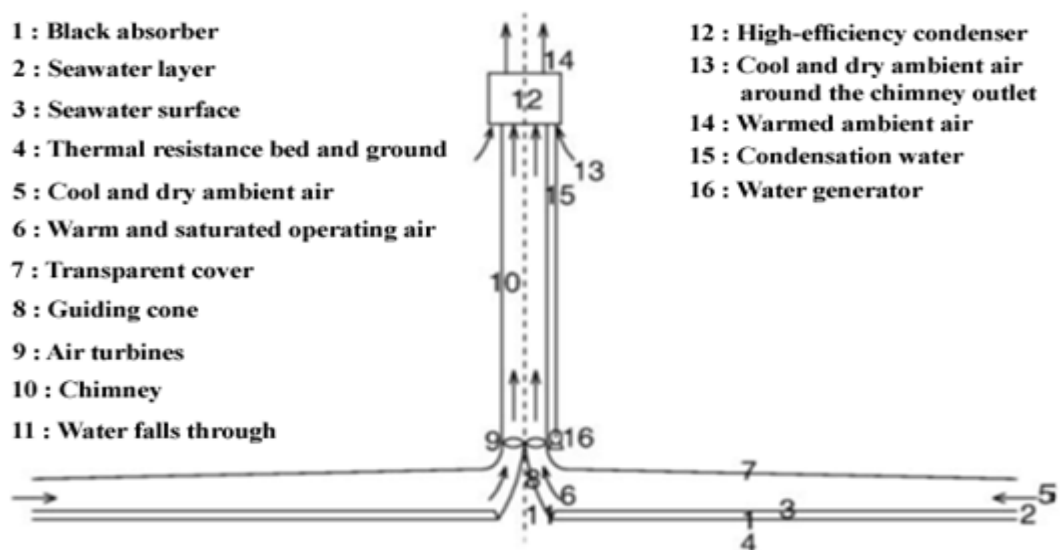


Figure 2.7: CSCSPD diagram [4].

Chapter 3

MATHEMATICAL MODEL

In this study, a mathematical method is employed to estimate and evaluate the CSCSPD's performance. The mathematical model developed utilizing MATLAB software was used to compute the performance of the integrated system.

The components of CSCSPD system include the solar collector, the turbine generator, the solar chimney and the HEC.

In the proposed plant system, the dry ambient air becomes warm and saturated when it streams through a layer of seawater drawn from the adjacent sea. When warm saturated air rises from the bottom to the top of the chimney, the temperature decreases, and a small quantity of vapor is condensed to fresh water. The fresh water descends from a considerable height in the chimney and is gathered in a trough placed in the bottom around the guiding cone. The fresh water in the bottom trough is then withdrawn continuously. The warm and saturated air enters directly into the high-efficiency condenser after flowing out from the chimney. The cold ambient air around the chimney outlet naturally enters the condenser due to a difference in pressure. The condenser needs to be placed at the top of the chimney. In the designed condenser, the cold ambient air at the chimney outlet altitude allows for the vapor contained in the saturated air to condense and so produce fresh water. This condensation occurs naturally and needs no additional energy. The effect of the highly efficient condenser

on the flux out of the up-drafting air in the solar chimney is usually not noticeable. The fresh water falls and drives the water generators installed above the collector to generate electricity and convert the gravitational potential energy of water into electric power. After this simple procedure, a small quantity of fresh water can be drawn-out from the low trough and a huge fall from the water generator will supply fresh water to fulfill local needs.

This new system has a twofold production advantage. Quantities of freshwater are produced by vapor condensate on the walls of the chimney and vapor condensate into the HEC. Additionally, electrical energy is produced by an air-turbine inserted in the inlet of the solar chimney alongside the electric power produced by the generator itself. This very simple system facilitates the production of freshwater as well as the provision of electrical energy [4].

The chimney and the HEC are the main and only components that are discussed and evaluated in this study. To estimate the performance of these parts, the values estimated by Zhou et al for properties of the CSCSPD system, particularly at the chimney inlet [4] were used.

The mathematical model used is based on assumptions that can be divided into two parts. The first part entails assumptions governing the chimney and are as follows [4] [20]:

- 1- Ideal gas laws apply for operating air.
- 2- No area change, no internal obstructions.
- 3- The chimney walls are assumed to be slippery and adiabatic.
- 4- No additional losses, no heat transfer of work extraction.

- 5- The buoyant force outside the chimney in the system is neglected.
- 6- Performance of warm airflow through the turbine does not change.

The second part in the assumptions governing the model deal with designing the condenser at the chimney outlet in following manner [21]:

- 1- Steady operating conditions exist.
- 2- The condenser is well insulated, so that the heat loss to the surroundings is negligible and heat transfer from the humid air at the end of the chimney is equal to the heat transfer to the ambient air entering the condenser.
- 3- Changes in the kinetic and potential energies of fluid streams are negligible.
- 4- The overall heat transfer coefficient is constant and uniform.

The mean value time is taken as 86400s with solar radiation of 1000 w m^{-2} was used in energy calculations.

3.1 The Chimney

The solar chimney is the actual thermal engine of the power system. The chimney converts the hot saturated airflow into kinetic energy, which is determined by the temperature rise of the collector outlet airflow and the chimney height [22].

The chimney can be defined as an ideal chimney, if it has no area change, internal obstructions, wall friction or additional losses and no heat transfer or work extraction [20].

The one-dimensional compressible flow equation in the chimney can defined as follows [4] :-

State equation: -

$$dp/p = dT/T + d\rho/\rho \quad (3.1)$$

Where, p is the pressure, T is the temperature, ρ is the density.

Mass equation:-

$$d\rho/\rho + du/u = 0 \quad (3.2)$$

Where, u is the vertical velocity.

Momentum equation:-

$$dp + \rho u du + \rho g dz = 0 \quad (3.3)$$

Where, g is the gravity acceleration, z is any height.

Energy equation:-

$$-dh (\dot{m}(z) - \delta\dot{m}) + L \delta\dot{m} = (\dot{m}_f(z) - \delta\dot{m}) g dz \quad (3.4)$$

According to Zhou et al. [4] wet air (humid air) enters the chimney inlet at 38.9 °C and 7.58 m/s as inlet chimney vertical velocity, and it is assumed that the chimney inlet region is affected by sea level atmospheric pressure.

Vapor partial pressure can estimated by:-

$$P_v = \rho_v \cdot R_v \cdot T \quad (3.5)$$

With the density of vapor ρ_v , R specific gas constant of water vapor 461 J Kg⁻¹ K⁻¹, or vapor pressure can be taken from Hardy et al. [23].

As a function of specific humidity and atmospheric pressure, the partial pressure of water vapor can be estimated by the following equation [24]:-

$$P_v = P \cdot \frac{\omega}{0.622 + \omega} \quad (3.6)$$

Where, P_v is the vapor pressure, P is the atmospheric pressure, ω is the specific humidity.

The saturated pressure of wet air can be calculated as [24]:-

$$P_{sv_0} = P_{sv} / 10^{8.5(T-273.15)/T} \quad (3.7)$$

The saturated vapor pressure at 0 °C, P_{sv_0} is equal to 608.2 Pa. Relative humidity of wet air defined as [24]:-

$$RH = \frac{P_v}{P_{sv}} \quad (3.8)$$

The atmospheric density can specifically be express as [24]:-

$$\rho = \frac{P-RH}{R_d \cdot T} \frac{P_v}{P} + \frac{RH}{R_s \cdot T} \frac{P_v}{P} \quad (3.9)$$

The partial pressure of dry air can be calculated by subtracting atmospheric pressure of the region from vapor partial pressure [4]. By considering atmospheric pressure, the density of humid air can be expressed as [24]:-

$$\rho = \frac{P-P_v}{R_d \cdot T} + \frac{P_v}{R_s \cdot T} \quad (3.10)$$

The specific gas constant of dry air and specific gas constant of vapor is equal to 287 J kg⁻¹ K⁻¹ and 461 J kg⁻¹ K⁻¹ respectively.

The specific humidity of wet air can be estimated as [21]:-

$$\omega = \frac{\rho_v}{\rho_d} = 0.62198 \cdot \frac{P_v}{P-P_v} \quad (3.11)$$

The specific heat capacity of vapor at constant pressure (C_p) is estimated by the following equation [4]:-

$$C_p = 1880 \cdot \omega + 1010 \quad (3.12)$$

The specific enthalpy (h) of water vapor can be calculated by [4]:-

$$C_p T_0 = \frac{u^2}{2} + C_p T = h \quad (3.13)$$

Here, u is the vertical velocity in the chimney, T_0 is the stagnation temperature, so the specific enthalpy equation can be simplified as [4]:-

$$dh = \frac{L \delta \dot{m}}{\dot{m}_f} - g dz = \delta \dot{m}_f - g dz \quad (3.14)$$

The Mach number at the chimney inlet and outlet is a dimensionless quantity representing the ratio of the velocity of an object moving through a fluid and the local speed of sound can be expressed as [25]:-

$$\text{MACH} = \frac{\text{VELOCITY}}{\text{SPEED OF SOUND}} = \frac{u}{c} \quad (3.15)$$

In addition, the speed of sound can be estimated as [25]:-

$$C = \sqrt{K \cdot R \cdot T} \quad (3.16)$$

Where K is the ratio of specific heats, R is gas constant and T is the absolute temperature (K).

The static temperature of the chimney inlet can be estimated by [20]:-

$$T_1 = T_{01} / [1 + \text{Mach}_1^2 (K - 1)/2] \quad (3.17)$$

Mach_2 represent the Mach number at the chimney outlet [4]:-

$$\ln \text{Mach}_2 - \frac{1}{2} \text{Mach}_2^2 = \frac{r-1}{c_p^2} \Delta Q + \frac{g}{c_p^2} H_1 + \ln \text{Mach}_1 - \frac{1}{2} \text{Mach}_1^2 \quad (3.18)$$

The stagnation temperature of the chimney outlet airflow T_{02} can be estimated by the following equation as [4] :-

$$\frac{\Delta Q}{c_p} + T_{01} - \frac{g}{c_p} H_1 = T_{02} \quad (3.19)$$

Where, ΔQ is the total latent heat, T_{01} is the stagnation temperature at chimney inlet, T_{02} is the stagnation temperature at chimney outlet.

At the chimney outlet, the static temperature of the airflow calculated by [4]: -

$$T_{02} = T_2 * [\text{Mach}_2^2 (K - 1) / 2 + 1] \quad (3.20)$$

The static pressure of the atmosphere at a height (h) is expressed by [24]:-

$$P = P_0 \left(1 - \frac{0.0065 z}{T_0} \right)^{5.256} \quad (3.21)$$

The static temperature of the atmosphere at a height (z) expressed as a function of static temperature at the ground level T_0 and height using the relation at [24]:-

$$T = T_0 - 0.0065 z \quad (3.22)$$

The equation of atmospheric pressure can be modified to the following equation proposed by [4]:-

$$P = P_0 \left(1 - \frac{H_1}{44300} \right)^{5.256} \quad (3.23)$$

With P_0 being the static pressure at 0 m above sea level, and T_0 at 0 m above sea level equal to 288.15 K (15 °C) .

The operating air mass flow rate can be estimated by :-

$$\dot{m}_f = \rho \cdot A \cdot u \quad (3.24)$$

Where u is the vertical velocity at the inlet and outlet chimney respectively, A presented the chimney area equal to $\pi r^2 = 20106.192 \text{ m}^2$.

A relation between the atmospheric pressure at chimney inlet P_1 and the atmospheric pressure at chimney outlet P_2 as expressed by Zhou et al. [4] From the mass flow equation as the following:-

$$\frac{P_2}{P_1} = \frac{\text{Mach}_1}{\text{Mach}_2} \left(\frac{T_2}{T_1} \right)^{0.5} \quad (3.25)$$

The MFR of condensed water vapor in the chimney can be calculated by [4]:-

$$\dot{m}_{\text{water1}} = \dot{m}_{f_1} \frac{\omega_1}{1+\omega_1} - \dot{m}_{f_2} \frac{\omega_2}{1+\omega_2} \quad (3.26)$$

The chimney is the actual thermal engine of the power system. The chimney converts the hot air flow into kinetic energy that is actually determined by the temperature rise of the collector outlet airflow and the chimney height [24].

The pressure difference ΔP that is produced between the chimney base and the ambient is calculated by [4]:-

$$\Delta P = g \cdot \int_0^{H_1} (\rho_a(h) - \rho(h)) dh \quad (3.27)$$

with height, the density linear variation of air is proposed, ΔP is expressed by the following equation [4]:-

$$\begin{aligned} \Delta P &= g \cdot \int_0^{H_1} ((\rho_{a_1} - \rho_1) - (\beta_a - \beta)) dh \quad (3.28) \\ &= g \cdot ((\rho_{a_1} - \rho_1)H_1 - \frac{1}{2} (\beta_a - \beta)H_1^2) \end{aligned}$$

Where, β is the mean gradient of the air density inside the chimney, β_a is the mean gradient density of ambient air, H_1 is the chimney height, they are calculated by [4]:-

$$\beta = \frac{\rho_2 - \rho_1}{H_1} \quad (3.29)$$

And

$$\beta_a = \frac{\rho_{a_2} - \rho_0}{H_1} \quad (3.30)$$

The vertical velocity of humid air at the chimney inlet estimated by Zhou et al. [4] is 7.58 ms^{-1} by, can be calculated by the following equation:-

$$u_1 = \sqrt{\frac{2(1-n)\Delta P}{\theta \cdot \rho_1}} \quad (3.31)$$

According to Zhou et al. [4], n is considered to be 0.9 (constant), which is a factor of reduced pressure at the turbine. θ represent total pressure loss coefficient involving, wall friction factor $f = 0.008428$ chimney [22], entrance coefficient $\varepsilon_{in} = 0.056$ by

assuming the inlet guide vane angle and collector roof height are respectively 22.5° and 0.356° [22], and the exit loss coefficient of kinetic energy $\varepsilon_{out} = 1.058$ [22].

The power produced by the air turbine can be calculated by:-

$$\dot{W}_{at} = \eta_{at} n A_{ch} u_1 \Delta P \quad (3.32)$$

Schlaich assumed the efficiency of the air turbine generator (η_{at}) as 80 % [7].

3.2 High-Efficiency Condenser

The effectiveness-NTU method is more appropriate for selecting the suitable type of heat exchanger application, for determining any unknown inlet or outlet temperature and for the heat transfer rate using an energy balance.

The method is based on a dimensionless parameter called the heat transfer effectiveness ε , defined as [21]:-

$$\varepsilon = \frac{\dot{Q}}{Q_m} = \frac{\text{Actual heat transfer rate}}{\text{Maximum possible heat transfer rate}} \quad (3.33)$$

The maximum temperature difference in heat exchanged is the difference between the inlet temperature of the humid air and the ambient. This helps in determining the maximum possible heat transfer rate in the heat transmitter [21]:-

$$\Delta T_{max} = T_2 - T_{a2} \quad (3.34)$$

Where, T_2 is the temperature of operating air at chimney outlet, T_{a2} is the temperature of ambient air at chimney height. The heat transfer in a heat exchanger will reach to its maximum value when the hot fluid is cooled to the inlet temperature of the added fluid.

The maximum possible heat transfer rate in a condenser:-

$$\dot{Q}_m = CR_{min} \cdot \Delta T_{max} \quad (3.35)$$

Minimum heat ratio capacity CR_{min} is the smaller of the $CR_2 = \dot{m}_{f_2} \cdot C_{p_2}$ and $CR_{a_2} = \dot{m}_{a_2} \cdot C_{p_a}$.

The MFR of cold air at chimney height and HEC inlet expressed as [26]:-

$$\dot{m}_{a_2} = \dot{m}_g \cdot DF \quad (3.36)$$

where, \dot{m}_g is the MFR of ground ambient air (at sea level), DF is the density factor expressed by:-

$$DF = \frac{\rho_{a_2}}{\rho_g} \quad (3.37)$$

The mass flow rate of ambient air at the ground can be estimated by [21]:-

$$\dot{m}_g = \rho_g \cdot u_g \cdot A_{cond} \quad (3.38)$$

Where, ρ_g is density of ambient air at the inlet of the condenser corresponding to the ambient air temperature at chimney height. u_g is the average annual velocity of air at sea level in Dalian, China [27], A_{cond} is the cross sectional area of the HEC.

The estimation of \dot{Q}_m requires, the availability of the inlet temperature of hot and cold fluid and their MFR, once the effectiveness of the condenser is known the actual transfer rate \dot{Q} can be determined as [21] :-

$$\dot{Q} = \varepsilon \cdot \dot{Q}_m \quad (3.39)$$

The actual heat transfer rate in a condenser can be determine from an energy balance on the hot or cold fluids and can be expressed as [21]:-

$$\dot{Q} = CR_{a_2} (T_{a_3} - T_{a_2}) = CR_2 (T_2 - T_3) \quad (3.40)$$

the energy balance for HEC is expressed by [4]:-

$$CR_{a_2}(T_{a3} - T_{a2}) = CR_2(T_2 - T_3) \quad (3.41)$$

Where, T_{a3} is the temperature of ambient air at condenser outlet, T_{a2} is the temperature of the ambient air at condenser inlet .

The MFR of water vapor condensed to water in the HEC expressed by [4]:-

$$\dot{m}_{water2} = \left(\frac{\omega_2}{1+\omega_2} - \frac{\omega_3}{1+\omega_3} \right) \cdot \dot{m}_{f_2} \quad (3.42)$$

The power of the water generator is estimated by [4]:-

$$\dot{W}_{wg} = \eta_{wg} \dot{m}_{water2} g H \quad (3.43)$$

The efficiency of the water generator η_{wg} can reach 90 % [7].

The total electric power of (CSCSPD), \dot{W}_{total} which is equal to the sum of the \dot{W}_{at} generated from the turbine generator and \dot{W}_{wg} generated from the water generator, is expressed by [4] as:-

$$\dot{W}_{total} = \dot{W}_{at} + \dot{W}_{wg} \quad (3.44)$$

The output heat from the high efficiency condenser \dot{Q}_w can be estimated by the following equation:

$$\dot{Q}_w = h_{fg} \dot{m}_{water2} \quad (3.45)$$

The (CSCSPD) efficiency of total energy conversion η_{pp} is expressed by [4] as:-

$$\eta_{pp} = (\text{desired output}) / (\text{desired input}) = (\dot{W}_{total} \dot{Q}_w) / (A_{coll} I) \quad (3.46)$$

Based on the calculation mentioned above, which specializes with a mathematical model, a computation calculation has been done by (MATLAB) software to predict, estimate and analyze the performance of (CSCSPD).

Chapter 4

PARAMETERS AND RESULTS

This work is based on a theoretical 500m high power generating solar chimney with an inner diameter of 160m at a site, where the typical atmospheric condition is about 288.15 K and 101 kPa according to Zhou et al. [4]. The rise in temperature of the air at the collector outlet where turbines are on load assumed to be 23.9 °C, the wind velocity at sea level is 5 m s⁻¹ according to the meteorology of Dalian, China.

Table 4.1 shows the study parameters and results collected and estimated by a mathematical model for CSCSPD. The power output given is for the proposed plant being active for 24 hours a day, over a period of a full calendar year at a site with an average global solar radiation of 4.93 kWh m⁻² received by the collector during one day and 1800 kWh m⁻² is being the global solar radiation during a year.

Table 4.1: The parameters and results for CSCSPD.

Parameter	Value	Parameter	Value
Diameter of collector (m)	6000	Condenser diameter (m)	80
Chimney height (m)	500	Effectiveness of condenser (%)	90
Chimney radius (m)	80	Temperature of ambient air at the condenser inlet (°C)	11.75
Temperature of airflow at chimney inlet (°C)	38.9	MFR of ambient air at condenser inlet (kg/s)	116670.6
Chimney inlet airflow velocity (m/s)	7.58	MFR of condensed vapor in HEC (kg/s)	3378.223
MFR of contained vapor at chimney inlet airflow (kg/s)	7398.8	Atmospheric pressure at the condenser outlet (kPa)	94.54
MFR of operating air at chimney inlet (kg/s)	167941	Electric power output produced from turbine generators (MW)	39.2
MFR of condensed vapor in chimney (kg/s)	1162.15	Power produced from water generators (MW)	14.91
Atmospheric pressure at chimney outlet (KPa)	95.44	Total power output (MW)	54.11
Chimney outlet airflow Velocity (m/s)	7.66	Output heat from condensed vapor in the HEC (kJ/s)	10261243
MFR of operating air at chimney outlet (kg/s)	162805.9	Efficiency (%)	38.5

Mathematical models for the economic and technical analyses were developed. Power delivered and water produced at different operating parameters were estimated by using MATLAB software.

4.1 Variations with Collector Radius

The radius of solar collector was carried between 2000-4500 m. The most important analytical models for the solar collector have been presented by Schlaich (1995), Kröger and Buys (1999) [12], Gannon and Von Backström (2000), Hedderwick (2001) and Beyers et al. (2002), Kröger and Buys (1999), Kröger and Buys (2001) [28], Jing-yin Li and Peng-Hua Guo et al. [29]. Their studies and research for the solar collector concluded with the same results that were estimated in this study for the CSCSPD. The results indicate clearly that total power production was increased as the collector radius increases, see Fig 4.1.

The total electric power plant, the area of the solar collector and the atmospheric solar radiation, dominates the efficiency of CSCSPD. Therefore, increasing the radius of the solar collector directly effects the efficiency of the integrated system, as is shown in Fig 4.2.

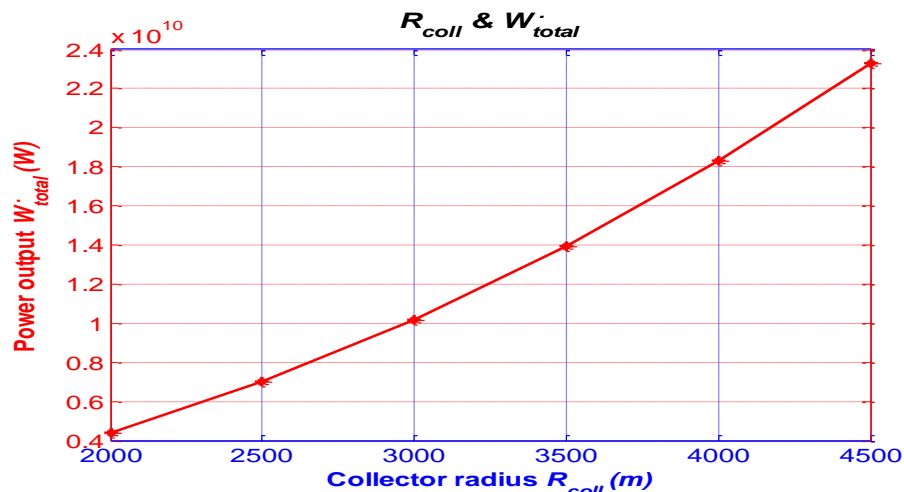


Figure 4.1: Variations of total electric power output from CSCSPD Vs. radius of solar collector.

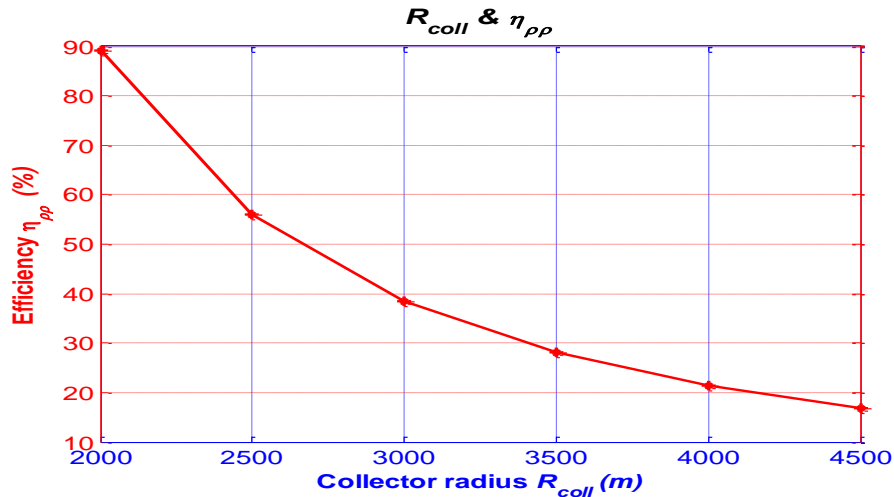


Figure 4.2: Variations of CSCSPD efficiency Vs. radius of solar collector.

4.2 Variations with Atmospheric Solar Radiation

The atmospheric solar radiation taken for this study was $1000\text{W}/\text{m}^2$. The short and long-wave solar radiation component was collected by the solar collector and transferred by heat convection to the operating air under the collector. The sea surface under the roof heated up and transferred the vapor radially, flowing above it from the outside to the chimney. Therefore, the increase in the solar radiation led to an increase in the total electric power, leading to a further increase in fresh water production from the solar chimney power plant, see Fig 4.3. This is one of the most important studies dealing with the effects of solar radiation on the flow presented by Huang et al. [10].

When, the atmospheric solar radiation decreases the efficiency of the integrated power plant increases according to the power plant efficiency equation see Equ 3.46. Thus, there is the estimated result mentioned above by MATLAB software due to the mathematical method for this study. These results are shown in Fig 4.4.

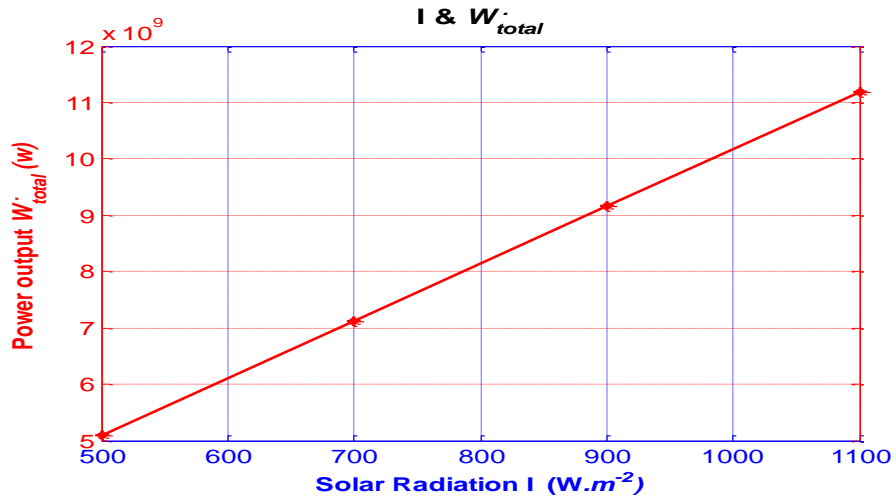


Figure 4.3: Variations of total electric power produced from CSCSPD Vs. atmospheric solar radiation.

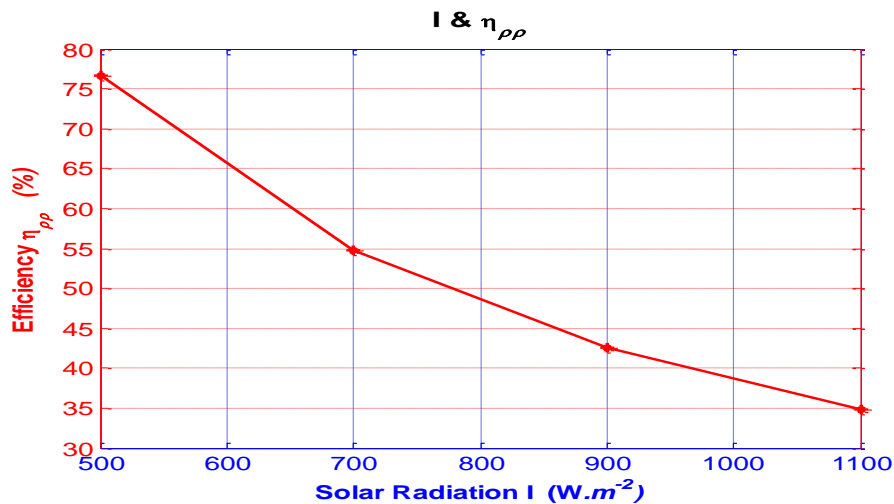


Figure 4. 4: Variations of CSCSPD efficiency Vs. atmospheric solar radiation.

4.3 Variations with MFR of Condensed Vapor at HEC

The saturated air passes through the chimney outlet and enters directly to the condenser inlet at an altitude of 500m. The hot saturated air is condensed in the HEC by heat transfer from cold ambient air entering the condenser at the same height. Figure 4.5 shows that as the mass flow rate of condensed vapor in the condenser increases, the amount of fresh water production increases. There is a similar increase in electric power produced from the water generator resulting in an overall increase

not only in total electric power but in the general efficiency of the power plant itself, see Fig 4.6.

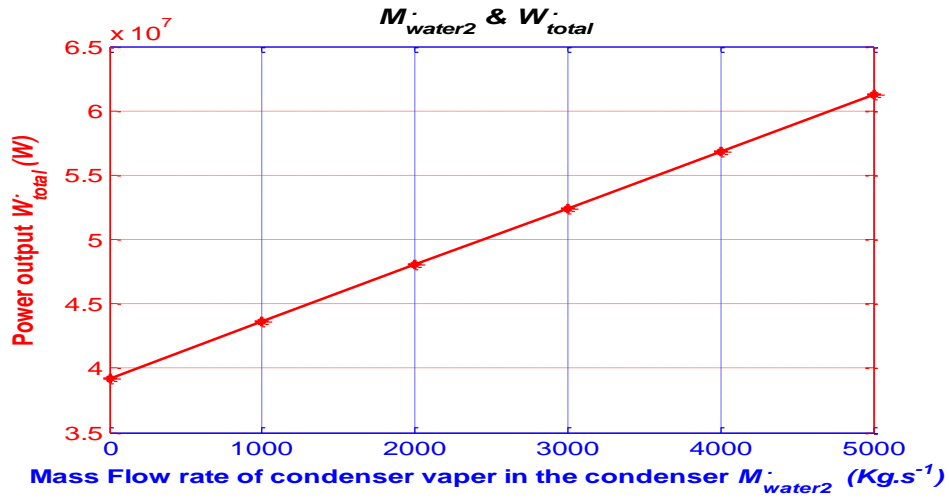


Figure 4.5: Variations of total electric output power from CSCSPD Vs. MFR of condenser condensed vapor.

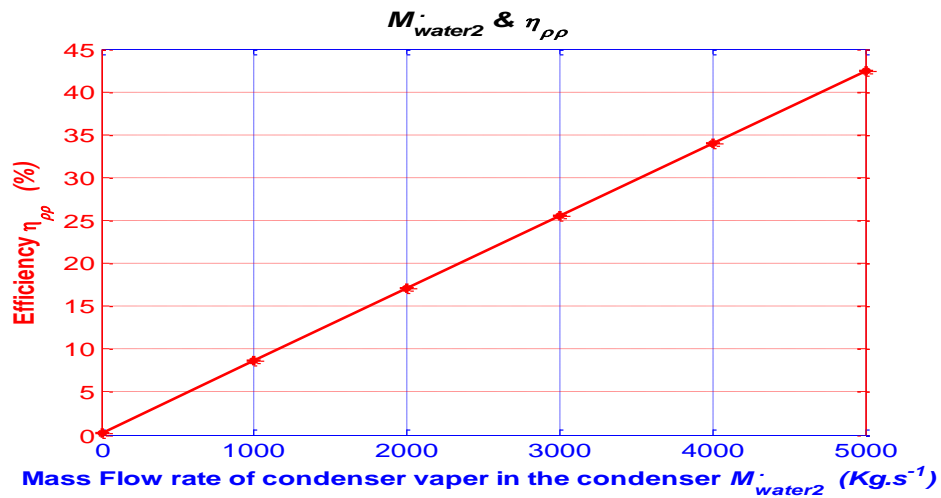


Figure 4.6: Variations of CSCSPD efficiency Vs. MFR of condenser condensed vapor.

4.4 Variations with Chimney Height

The chimney works as an effective thermal engine creating a temperature differential between the cool air at the condenser's inlet and the heated air at the bottom. This creates the chimney effect, which sucks air from the bottom of the tower out at the top.

The height of the chimney from the base to the condenser inlet H_1 is 500m as shown in Table 4.1. The electric power produced from the turbine generator, the total electric power produced from CSCSPD and the efficiency of the plant increased as chimney height was increased, see Fig 4.7 and Fig 4.8. Moreover, Jing-yin Li et al. [29], found similar results in their own research, concluding that an increase in the height of the chimney will bring about an increase in pressure difference between the ambient air and the air in the chimney.

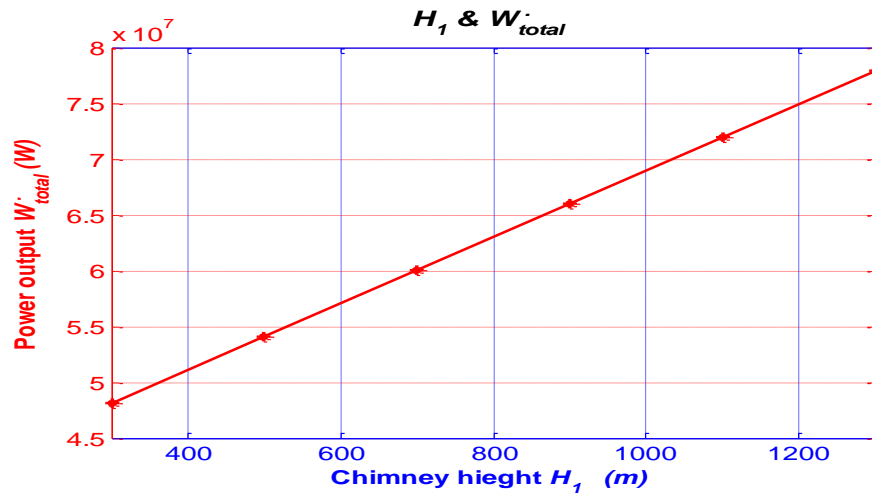


Figure 4.7: Variations of total electric power output from CSCSPD Vs. chimney height.

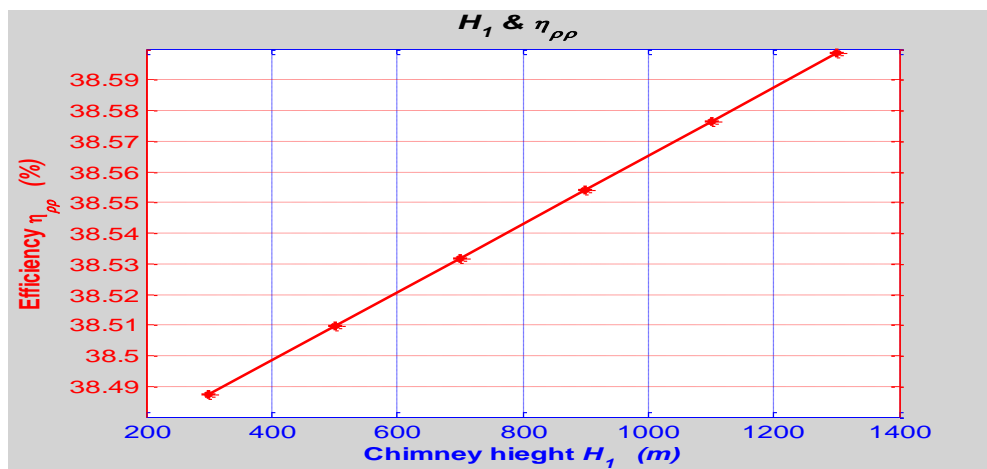


Figure 4.8: Variations of CSCSPD efficiency Vs. chimney height.

4.5 Variations with Chimney Radius

The chimney so described is considered as ideal because there is no change in its height as mentioned in the mathematical modeling assumptions. The area of the chimney is controlled by its diameter. The chimney's area affects many parameters in the power plant such as the mass flow rate of operating air through the chimney ($\dot{m}_{f_1}, \dot{m}_{f_2}$), the amount of fresh water production, the total electric power from CSCSPD affected by the chimney's area and the efficiency of the integrated power plant, see Fig 4.9. Figure 4.10 shows the results of the relation between the radius of the chimney and the efficiency of the CSCSPD. It is clear that as the chimney radius increased the total electric power output and the efficiency increases.

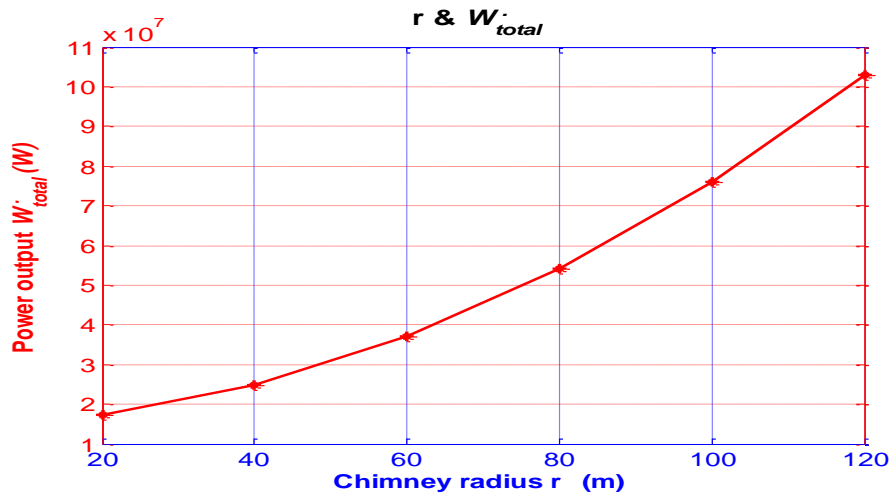


Figure 4.9: Variations of total electric power output from CSCSPD Vs. chimney radius.

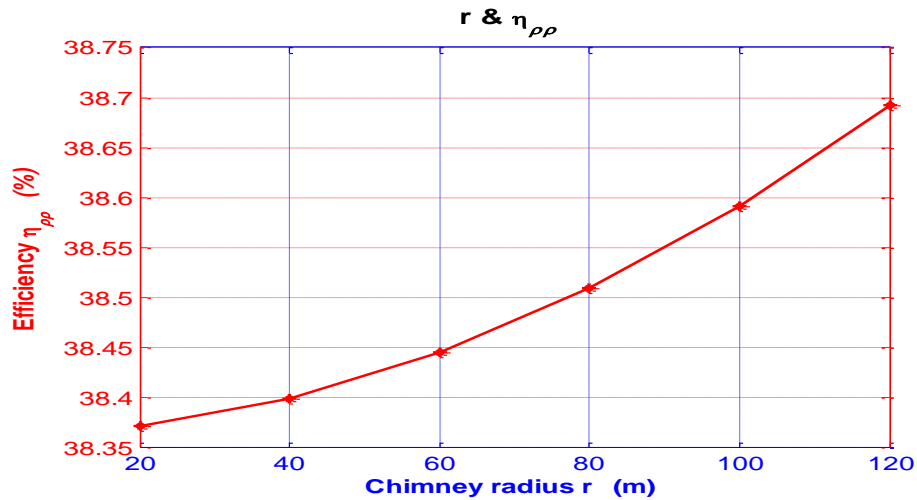


Figure 4.10: Variations of CSCSPD efficiency Vs. chimney radius.

4.6 Variations with Pressure Difference

The pressure difference between the chimney base and the ambient pressure at the outlet can be estimated from the density difference. This depends upon the temperature of the air at the inlet and at the top of the chimney. The pressure difference is available to drive the air turbine generator [28], which means that the increase in pressure difference and the increase in the air velocity is used to rotate the air turbine at the chimney base. An increase in electric power is produced by the air turbine generator increasing the total electric power and the power plant's efficiency from CSCSPD, see Fig 4.11 and Fig 4.12.

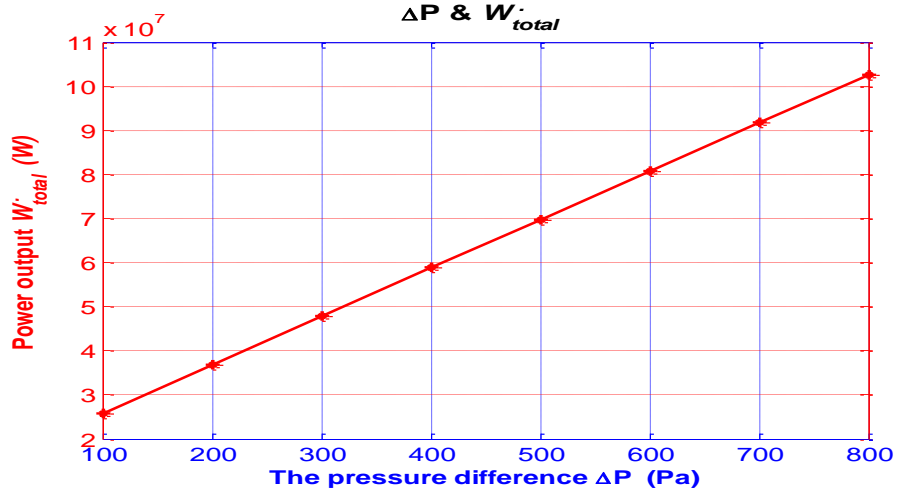


Figure 4.11: Variations of total electric power output from CSCSPD Vs. pressure difference.

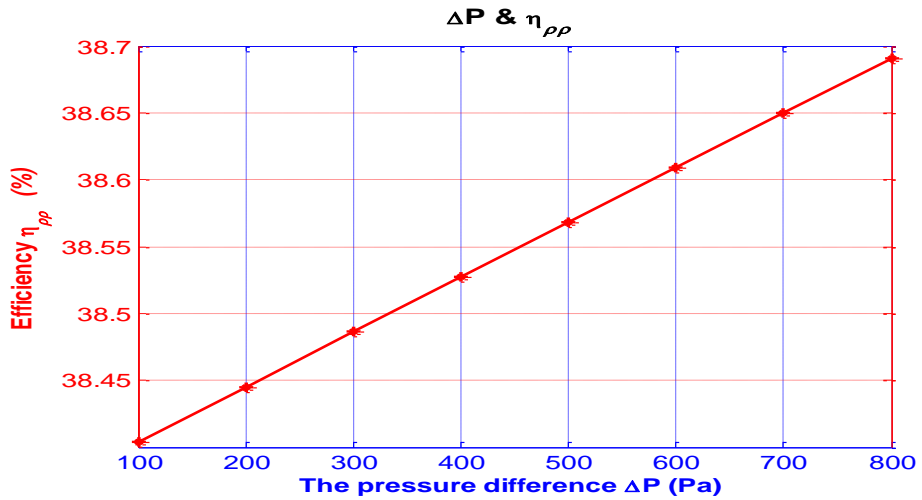


Figure 4.12: Variations of CSCSPD efficiency Vs. pressure difference.

4.7 Variations with Inlet Chimney Velocity

The velocity of the saturated operating air at the chimney inlet is 7.58 m/s as shown in Table 4.1. Figure 4.13 shows the consensual relationship between the air velocity at the chimney inlet and the total electric power produced from CSCSPD. Figure 4.14 shows the same type of relationship between the operating air at the chimney inlet and the efficiency of integrated power plant.

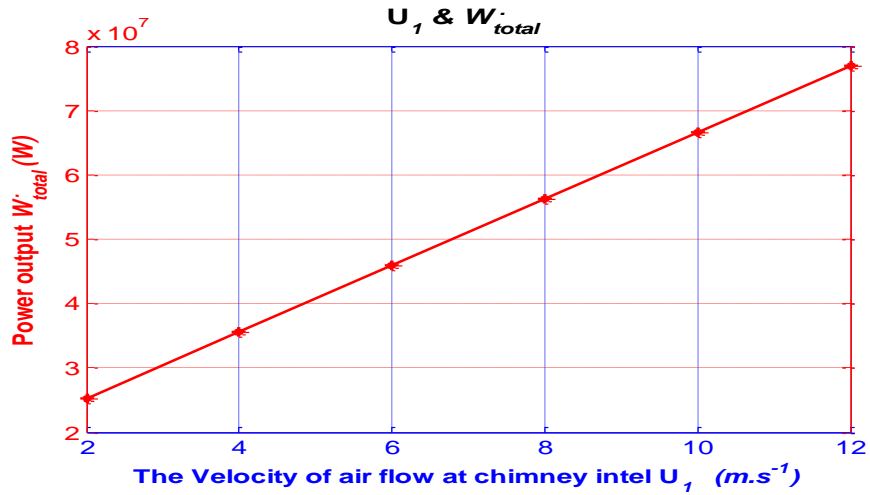


Figure 4.13: Variations of total electric power output from CSCSPD Vs. inlet chimney velocity.

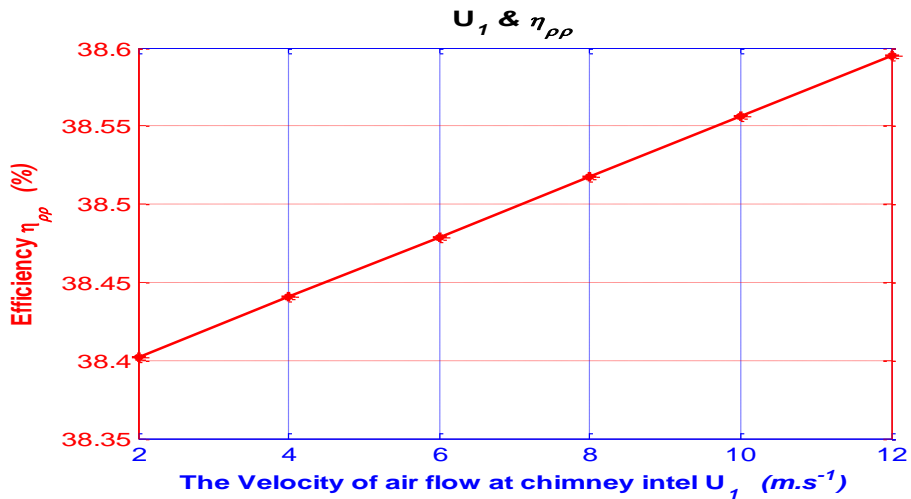


Figure 4.14: Variations of CSCSPD efficiency Vs. inlet chimney velocity.

4.8 Variations with Effectiveness of Condenser

The effectiveness of the condenser ϵ is a very important parameters for the heat transfer between the cold ambient air and the hot saturated air at the condenser inlets, the quantity of fresh water and electric power produces from water generator. Figure 4.15 shows the relation between the effectiveness of the condenser and the mass flow rate of the condensed vapor in the condenser. From Fig 4.16 and Fig 4.17 it can be seen

that the total electric power and the efficiency of the plant varies linearly with effectiveness of the condenser.

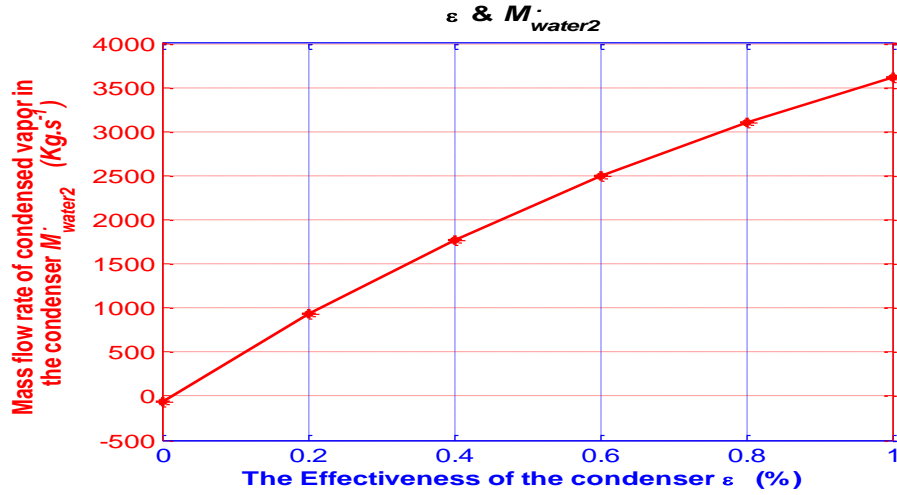


Figure 4.15: Variations of the MFR of condensed vapor in the HEC Vs. its effectiveness.

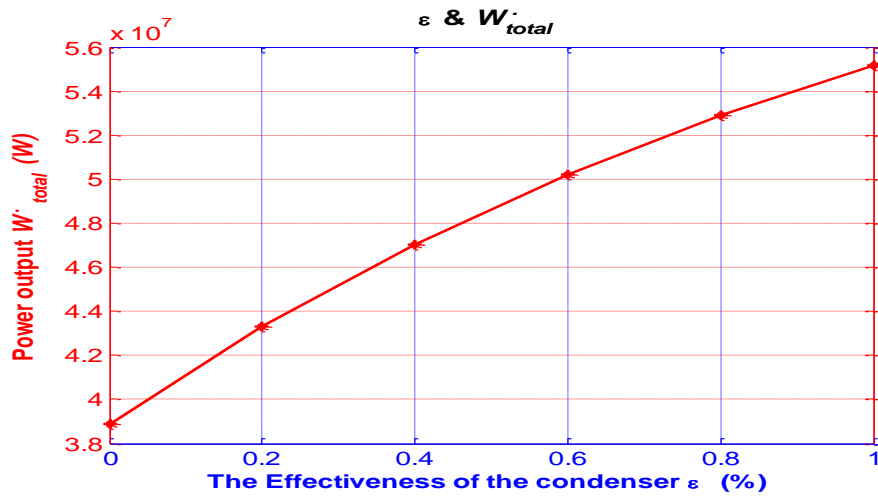


Figure 4.16: Variations of total electric power output from CSCSPD Vs. effectiveness of the condenser.

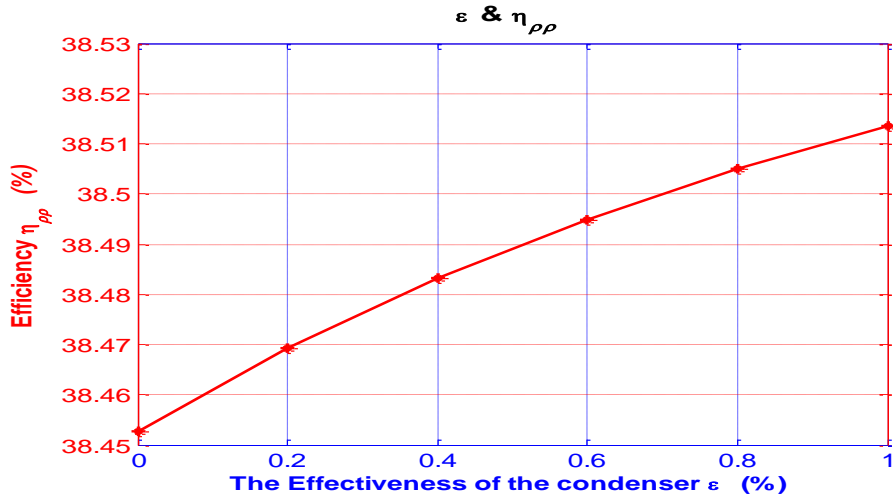


Figure 4.17: Variations of CSCSPD efficiency Vs. effectiveness of the condenser.

4.9 Variations with Mass Flow Rate of Ambient Air at Condenser

Inlet

Ambient air at 500m altitude enters the condenser inlet at a temperature of 11.75 °C, corresponding to atmospheric pressure of 95.44 kPa [30] as shown in Table 4.1. The increase for MFR of ambient air entering in the HEC causes more heat transfer from hot air flowing out of the chimney. This, in turn, produces more fresh water, more electric power from the water generator and more total electric power is produced from CSCSPD, as shown in Fig 4.18. The CSCSPD efficiency is shown in Fig 4.19.

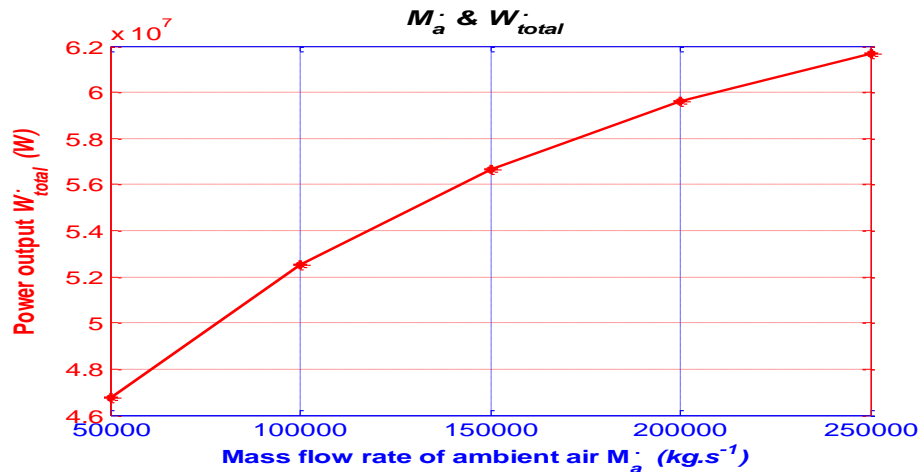


Figure 4.18: Variations of total electric power output from CSCSPD Vs. mass flow rate of ambient air at condenser inlet.

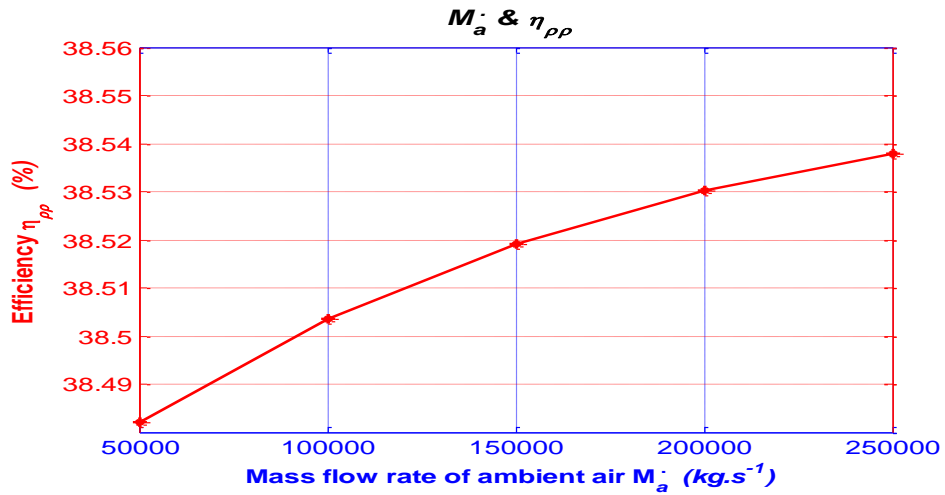


Figure 4.19: Variations of CSCSPD efficiency Vs. mass flow rate of ambient air at condenser inlet.

4.10 Variations with Condenser Radius

The large-scale condenser is used in this method to produce large quantities of fresh water. The radius of the condenser's cross sectional area must be taken into consideration alongside the estimation of the atmospheric pressure at the condenser outlet P3 (i.e. chimney height and condenser's diameter as well). With this method, the radius of the condenser is equal to the chimney's diameter, as shown in Table 4.1. From Fig 4.20 and 4.21 it can be seen that the total electric power and the efficiency of the plant varies linearly with radius of the condenser.

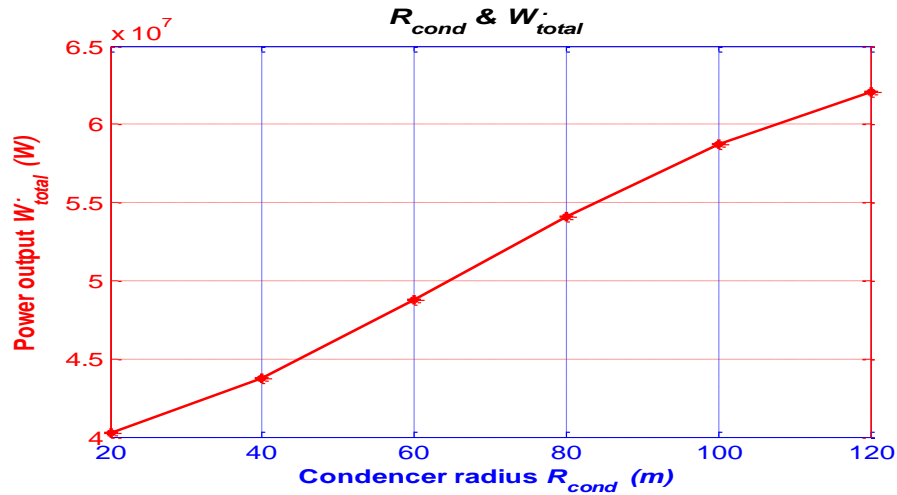


Figure 4.20: Variations of total electric power output from CSCSPD Vs. condenser radius.

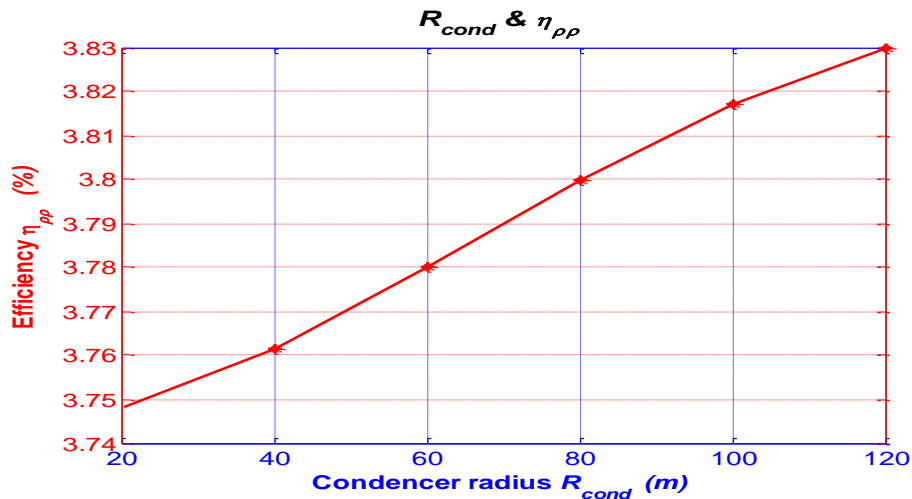


Figure 4.21: Variations of CSCSPD efficiency Vs. condenser radius.

4.11 Variations of Mach number at Chimney Outlet

Gannon & von Backström studied and examined many compressible flow models for an integrated power plant chimneys [28]. At the chimney outlet, the Mach number increased due to the increase in the velocity and the atmospheric pressure at the chimney outlet. From Fig 4.22 and 4.23 it can be seen that the total electric power and the efficiency of the plant varies linearly with Mach number at chimney outlet.

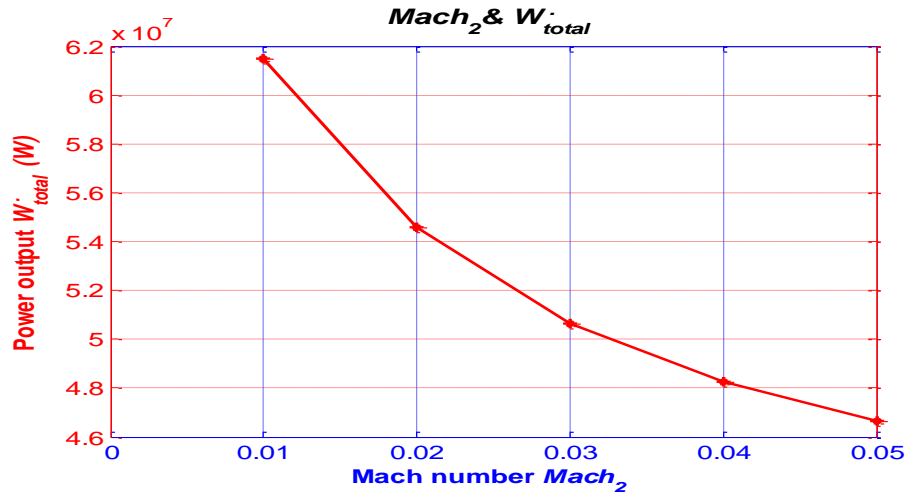


Figure 4.22: Variations of total electric power output from CSCSPD Vs. Mach number at chimney outlet.

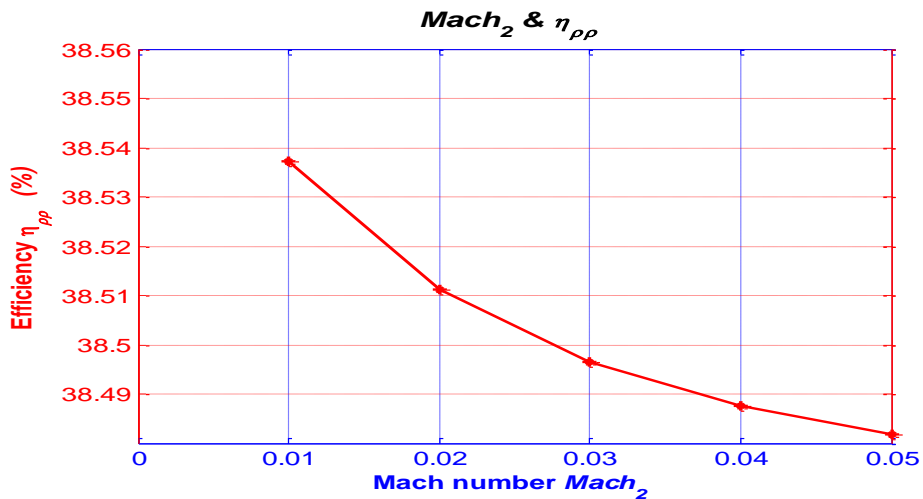


Figure 4.23: Variations of CSCSPD efficiency Vs. Mach number at chimney outlet.

4.12 Variations with Total Latent Heat

One of the important studies that deals with the effect of latent heat on the performance of a CSCSPD power plant is presented by Zhou et al. [24]. From Fig 4.24 and 4.25 it can be seen that the total electric power and the efficiency of the plant varies linearly with total latent heat.

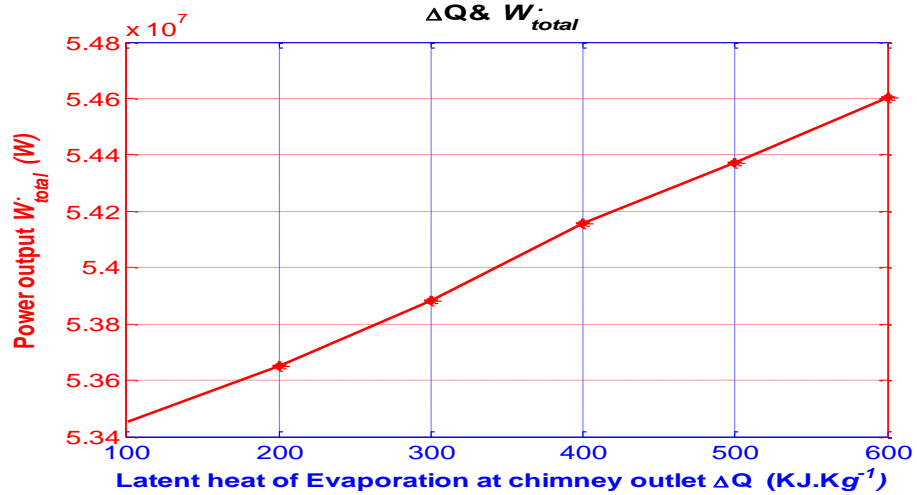


Figure 4.24: Variations of total electric power output from CSCSPD Vs. total latent heat.

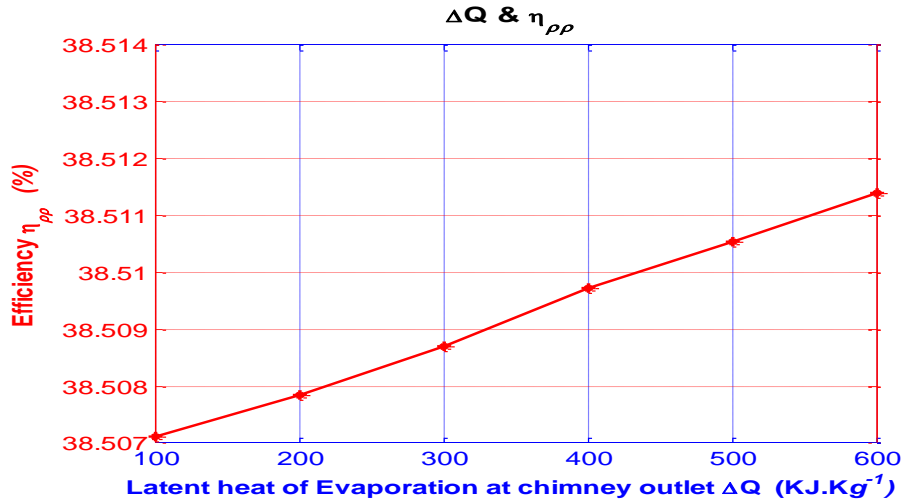


Figure 4.25: Variations of CSCSPD efficiency Vs. total latent heat.

4.13 Variations with Mass Flow Rate of Operating Air at Chimney

Outlet

The mass flow rate of operating air at the chimney outlet is determined by the parameters at the chimney outlet that contains the temperature, pressure and velocity, while the area of the chimney remains constant at the outlet as it is considered as an ideal chimney. Figure 4.26 shows the power output Vs. the mass flow rate of operating air at the chimney outlet. Figure 4.27 shows the efficiency of the CSCSPD Vs. the

mass flow rate of operating air at the chimney outlet. From Fig 4.26 and 4.27 it can be seen that the total electric power and the efficiency of the plant varies linearly with MFR of operating air at chimney outlet.

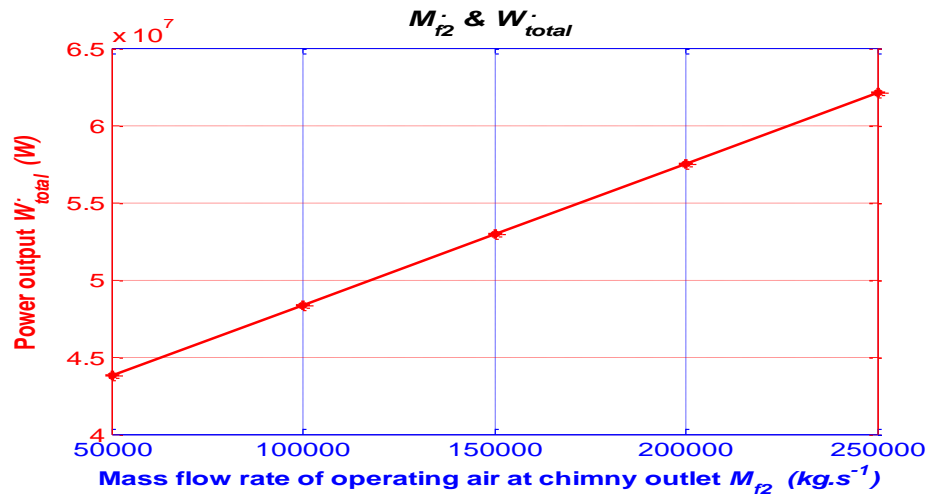


Figure 4.26: Variations of total electric power output from CSCSPD Vs. mass flow rate of operating air at chimney outlet.

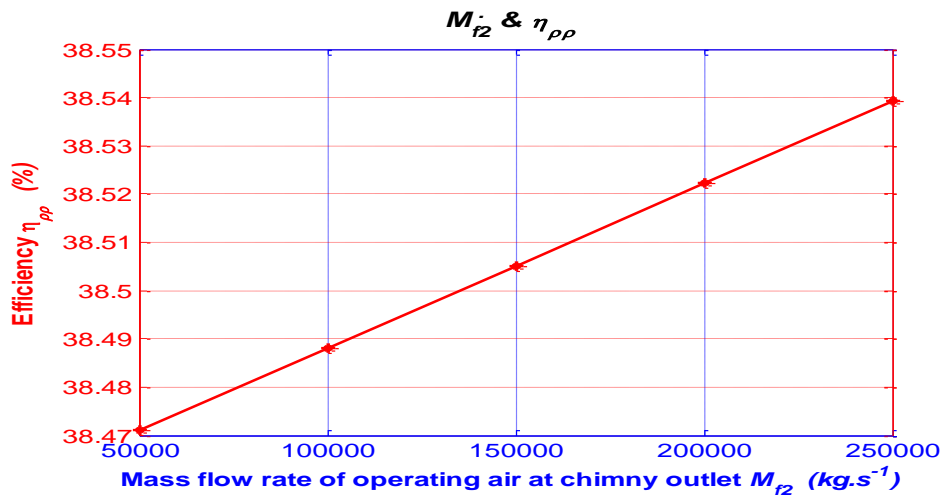


Figure 4.27: Variations of CSCSPD efficiency Vs. mass flow rate of operating air at chimney outlet.

4.14 Variations with Maximum Difference in Temperature between Operating Air and Ambient Air at Condenser Inlets

The maximum difference between the temperature of cold ambient air at chimney height and hot saturated air at the chimney outlet occurs at the condenser inlets. This parameter has significant importance for maximum heat transfer between fluids inside the condenser and for water production. Figure 4.28 shows the power output Vs. the maximum temperature difference. Figure 4.29 shows the efficiency of the CSCSPD Vs. the maximum temperature difference. From Fig 4.24 and 4.25 it can be seen that the total electric power and the efficiency of the plant varies linearly with the maximum temperature difference.

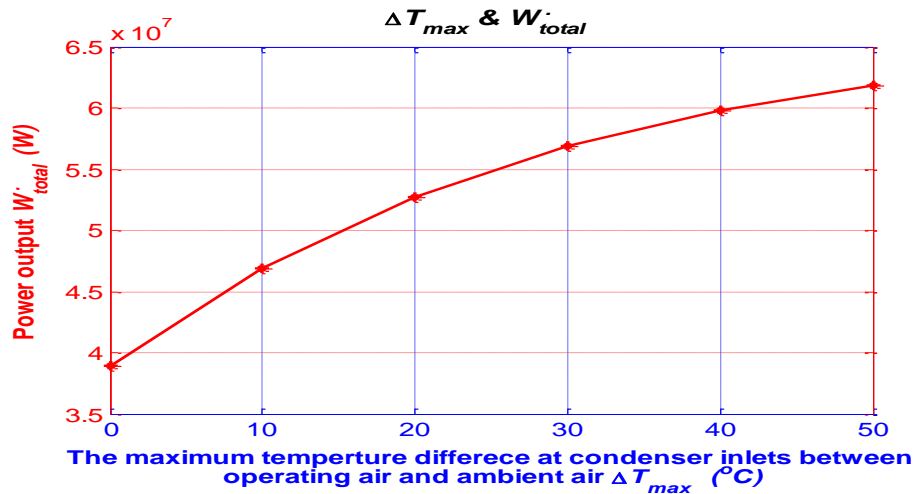


Figure 4.28: Variations of total electric power output from CSCSPD Vs. maximum difference in temperature between operating air and ambient at air condenser inlets.

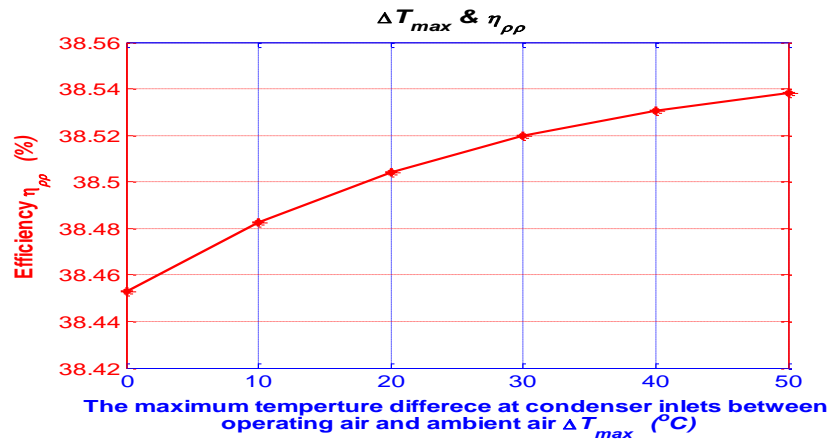


Figure 4.29: Variations of CSCSPD efficiency Vs. maximum difference in temperature between operating air and ambient air at condenser inlets.

4.15 Variations with Efficiency of Air Turbine Generator

Schlaich et al. [7] recommend that the efficiency of the air turbine generator η_{at} is equal to 80% as defined in this study. The efficiency of air turbine is the most important for the electricity production. From Fig 4.30 and 4.31 it can be seen that the total electric power and the efficiency of the plant varies linearly with the efficiency of air turbine.

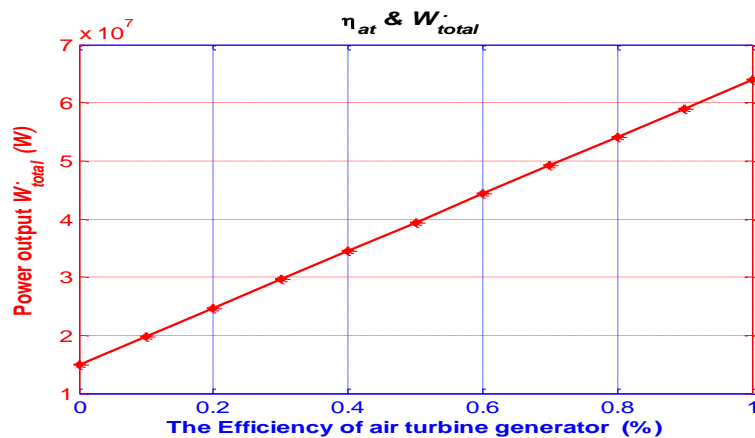


Figure 4.30: Variations of total electric power output from CSCSPD Vs. efficiency of air turbine generator.

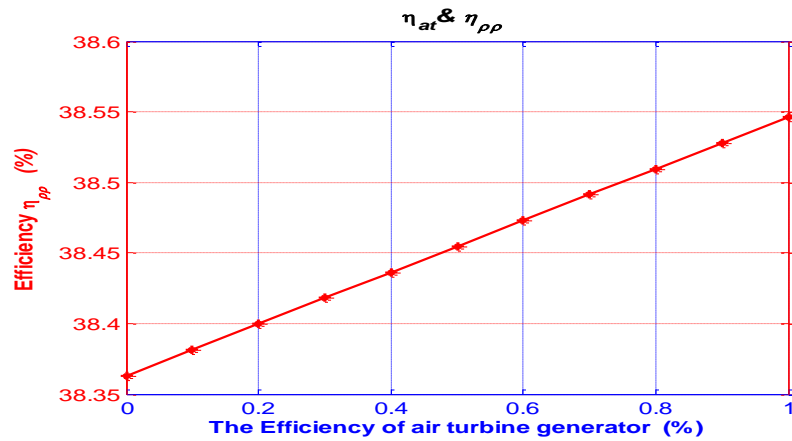


Figure 4.31: Variations of CSCSPD efficiency Vs. efficiency of air turbine generator.

4.16 Variations with Efficiency of Water Generator

The efficiency of the water generators η_{wg} are assumed as 90% [7]. The increase in the total electric power that occurred due to the increase in the efficiency of the water generator From Fig 4.32 and 4.33 it can be seen that the total electric power and the efficiency of the plant varies linearly with the efficiency of water generator.

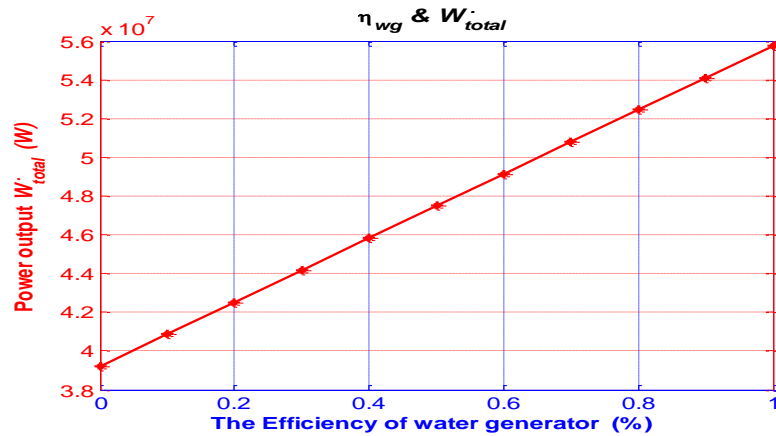


Figure 4.32: Variations of total electric power output from CSCSPD with Vs. efficiency of water generator.

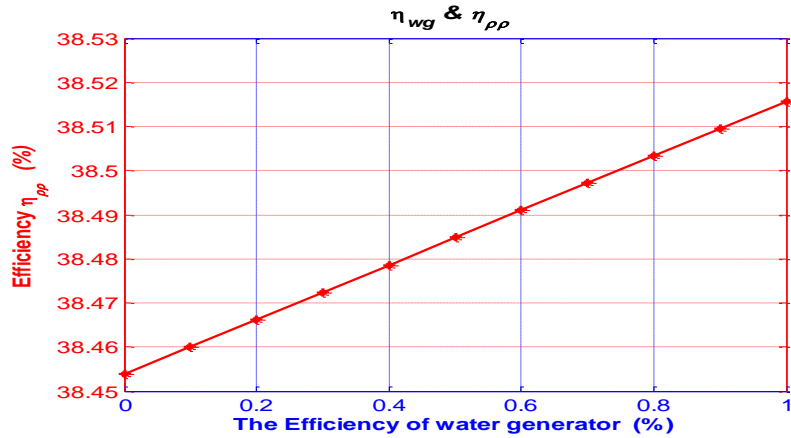


Figure 4.33: Variations of CSCSPD efficiency Vs. efficiency of water generator.

4.17 Variations of CSCSPD efficiency with total electric power output from CSCSPD

The total electric power produced from the integrated power plant represents the sum of the electric power produced by a turbine placed at the base of the chimney and the power generated from the water generator placed at the end of the condenser drainpipe. This consensual relation summarizes the most important parameters in this type of power plant as shown in Fig 4.34.

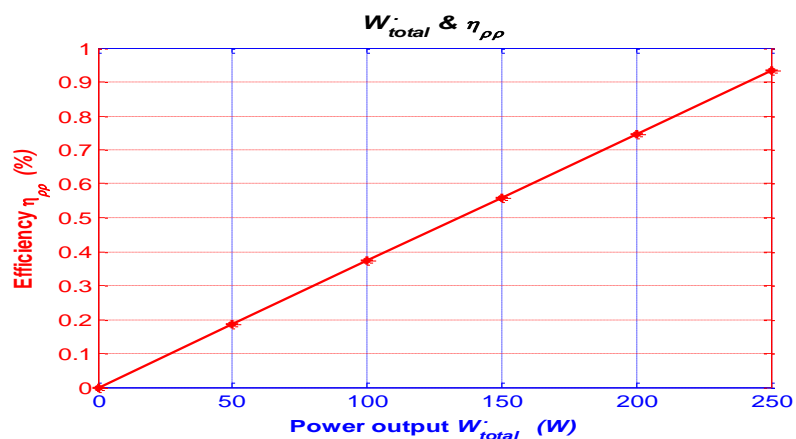


Figure 4.34: Variations of CSCSPD efficiency Vs. total electric power output from CSCSPD.

Chapter 5

ECONOMIC ANALYSIS

International concerns about the environment and the escalating demands for energy, coupled with steady progress in renewable energy technologies are now opening up new opportunities for the utilization of renewable energy resources. Solar energy is the most abundant, inexhaustible and cleanest of all the renewable energy resources available today.

The power from the sun intercepted by the earth is about 1.8×10^{11} MW, which is many times larger than the present rate of all energy consumption [31].

Solar chimney thermal power technology that has a long life span, promises large-scale solar power generating technology [32].

The CSCSPD is significantly valuable for energy and fresh water production to be used by both the public and by the industrial sector. For this reason alone, it deserves a broad economic analysis of the benefits of its use compared to other solar desalination systems.

Haaf et al. [10] assessed the relationship between the physical principles on the one hand and the scale and construction costs on the other. This economical power generation will also be possible with large-scale plants, designed with up to 400 MW.

The cost models for large-scale solar chimney power plants, were presented by Schlaich (1995), Schlaich (2004) and Bernardes (2004) [33].

Schlaich (1995) provides the price values for all plant components for plants of different sizes. He presented a procedure to evaluate the levelised electricity cost (LEC), investigated the sensitivity of the LEC to the interest rate and the length of the depreciation period [33].

Schlaich (2004) discussed the component cost and the LEC for various plants for fixed economic parameters. Bernardes (2004) presented a study similar to the one conducted by Schlaich (1995), calculated the cost of plants of various sizes and also proposed a procedure to evaluate the LEC and investigate the sensitivity of the LEC for the economic parameters. In addition to that, he derived a parametric cost model for the main plant components (collector, chimney and the power conversion unit) [33].

Pretorius & Kröger (2008) undertook a study to establish thermo economically optimal plant configurations for a large-scale SCPP. For that, an approximated cost model was developed, that provided the capacity for finding the optimum plant dimensions for different cost structures. The thermo-economically optimal plant configurations were obtained through multiple computer simulations and the results were compared to the approximated cost of each specific plant [12].

A study developed by Fluri (2009), revealed that previous economic models might have undervalued the initial cost of the levelised electricity of a large-scale solar chimney power plant. It also showed that carbon credits could significantly reduce the levelised electricity cost of such a plant [12] .

An economic analysis presented by Zuo et al. [2] was based on the two mathematical models. These models were developed individually for a one-dimensional flow in a solo solar chimney power system and a new solar chimney power system with the integration of seawater desalination. It was clear from this study that the economic benefits were significant.

Many countries around the world have developed plans to generate a certain percentage of their electricity capacity from renewable energy resources [34]. Many important economic steps can be implemented to reach these percentages including the provision of soft loans to buy and install these systems, leniency in tax programs and the payment for a unit price of electricity produced and fed into the main power grid for the region is higher [34] [35].

The operations and maintenance costs are considered negligible for these projects powered by solar energy; therefore, a large number of countries are supporting these projects economically [2].

5.1 Economic Model

An economic model based on a mathematical model of the integrated power plant is presented in this thesis. This economic model for CSCSPD is based on the following equations:

The cost of the integrated power plant can initially calculate by-

$$F_{pp} = \frac{\pi}{4} (D_{coll}^2 - D_{ch}^2) \times \frac{\epsilon_{coll}}{m^2} + \pi D_{ch} H_{ch} \times \frac{\epsilon_{ch}}{m^2} + \epsilon_{at} + \frac{\pi}{4} D_{cond}^2 \times \frac{\epsilon_{cond}}{m^2} \quad (5.1)$$

Where, F_{pp} is the cost of the CSCSPD, D_{coll} is the diameter of the solar collector, D_{ch} is the diameter of the chimney, ϵ_{coll} is the price of the collector, H_{ch} is the height

of the chimney, €_{ch} is the price of the chimney, €_{at} is the price of air turbine, D_{cond} is the diameter of the condenser, €_{cond} is the price of the condenser. Ref. [2] adopts a price system which contributes to simplify the process of economic analysis for the CSCSPD system (chimney: 250 €/m²; wind turbine generator: 0.5 M €; solar collector: 9 €/m²) and HEC in this study is assumed to be 18 €/m². These prices include the material price, the material transfer price and the construction price [2].

The service life (n) at least takes for 25 years, annual interest rate (i) is 6.2% [2], and the annuity coefficient estimated by:-

$$\xi = i(1 + i)^n / [(1 + i)^n - 1] \quad (5.2)$$

the average of annual investment calculated by:-

$$F_{yr} = F_{pp} \times \xi \quad (5.3)$$

If the operation period of the CSCSPD is taken at 24 h every day [4], the annual power output is calculated by the following equation:-

$$\dot{W}_y = \text{no. of days during a year} \times \dot{W}_{total} \quad (5.4)$$

The price of electricity is taken as 0.3 €/kWh [2], revenue received by the annual power output is estimated by:-

$$E_{power} = \text{the price of electricity} \times \dot{W}_y \quad (5.5)$$

The annual productivity of freshwater is estimated by the following:-

$$m_{water} = \text{no. of days during a year} \times \text{running hours in a day} \times 3600 \times (\dot{m}_{water1} + \dot{m}_{water2}) \quad (5.6)$$

Unlike a conventional coal-fired power plant, almost no greenhouse gas (GHG) is in the operation of the integrated system. Carbon dioxide (CO₂) equivalent released from the coal-fired power plant is calculated to be 0.95 kg CO₂ emissions kWh of electricity from coal as reported by [2]. The CO₂ emission reduction quantity is calculated by:-

$$M_{co_2} = (0.95 \dot{W}_y) \quad (5.7)$$

The price of credit carbon is 21.4 €/ton [2], possible credit carbon revenue is calculated by the following equation:-

$$E_{co_2} = 21.4 M_{co_2} \quad (5.8)$$

It is possible to calculate the price of fresh water by using the following equation:-

$$COST_{water} = (F_{yr} - E_{co_2} - E_{power}) / (M_{water} / \rho_{water} \times 10^{-3}) \quad (5.9)$$

The payback period is the time in which the initial cash outflow of an investment is expected to recover from the cash inflows generated by the investment. It is one of the simplest investment appraisal techniques and it is defined as:

$$Payback\ Period = \frac{Initial\ Investment\ Cash}{Inflow\ per\ Period} = \frac{F_{pp}}{E_{water} + E_{W_y}} \quad (5.10)$$

the previous equations represent the economic model for CSCSPD, the economic model written in the MATLAB software program is used to estimate the output parameters .

5.2 Variations with Collector Radius

The radius of the collector dominates the area of the solar collector. An increase in the diameter of the collector leads to an increase in the annual total power output. The annual revenue of electricity and the annual price of fresh water production Vs. collector radius are shown in Fig 5.1 and Fig 5.2 respectively. From Fig 5.1 and 5.2 it can be seen that the annual revenue of electricity and annual price of fresh water production varies linearly with radius of the collector.

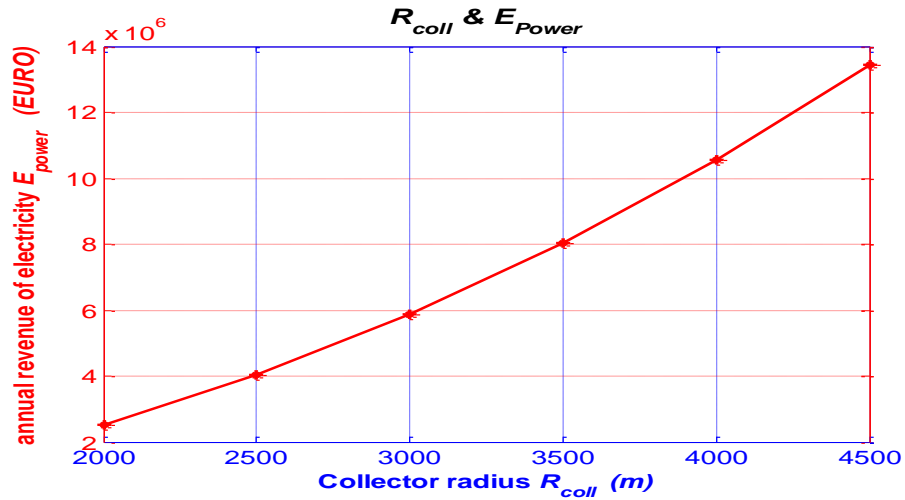


Figure 5.1: Variations of annual revenue of electricity Vs. collector radius.

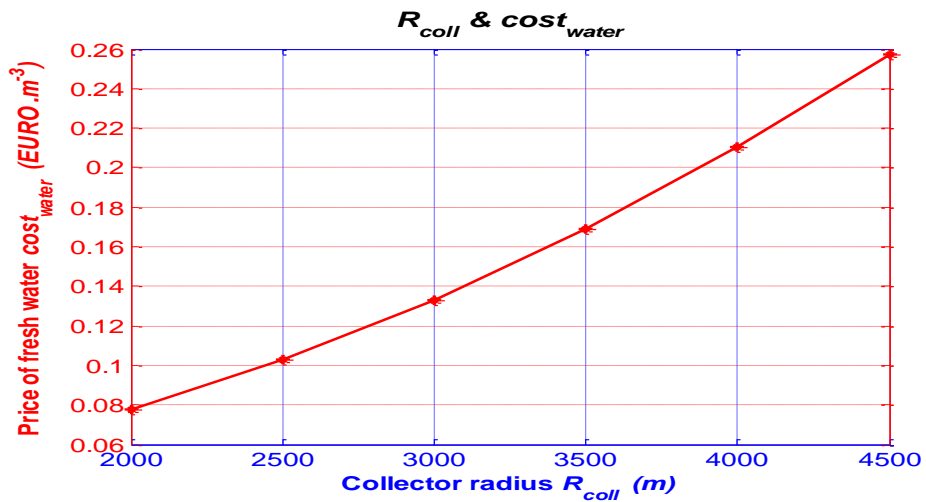


Figure 5.2: Variations of annual price of fresh water production Vs. collector radius.

5.3 Variations with Chimney Height

Height of chimney dominate the surface area of the chimney, the increase in chimney height leads to increase in the annual total power output, the annual revenue of electricity and annual price of fresh water production are shown in Fig 5. 3 and Fig 5.4.

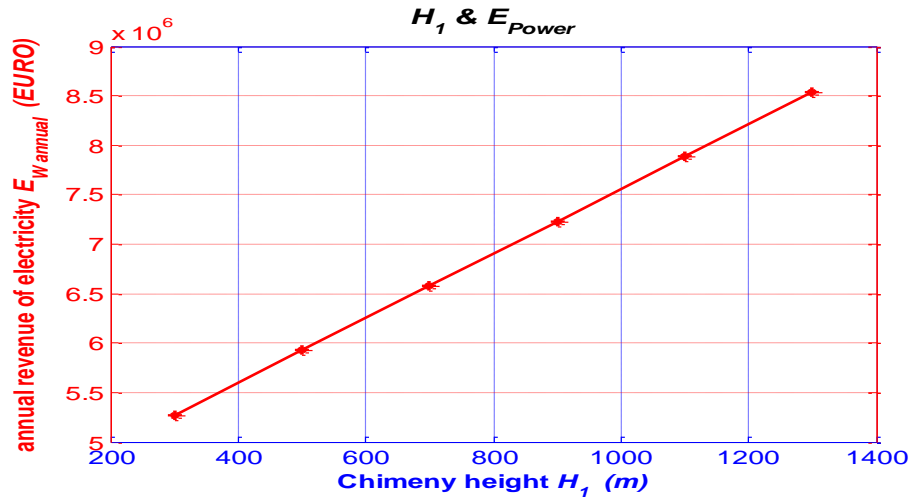


Figure 5.3: Variations of annual revenue of electricity Vs. chimney height.

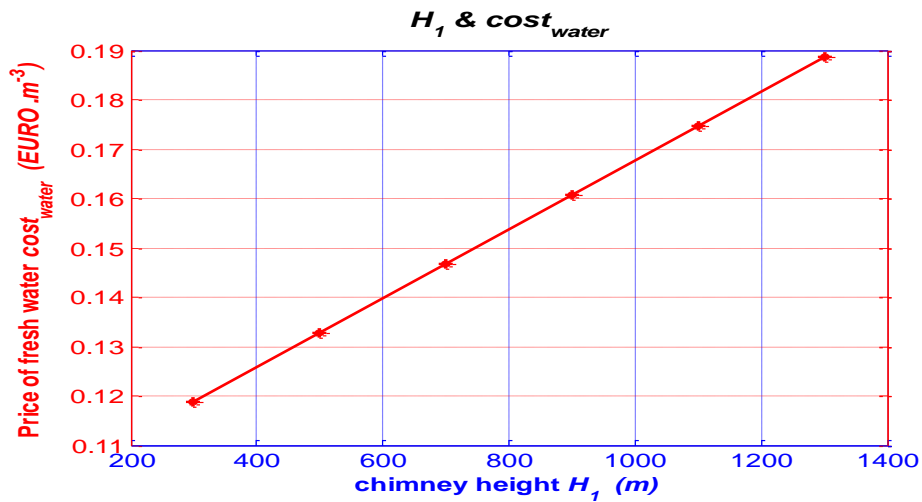


Figure 5.4: Variations of annual price of fresh water production Vs. chimney height.

5.4 Variations with Service Life

The service life of CSCSPD is significant for economic analysis. The increase in the years of service life affects the increase in the annuity coefficient. The annual average investment and the annual price of fresh water production are shown in Fig 5.5 and Fig 5.6 respectively.

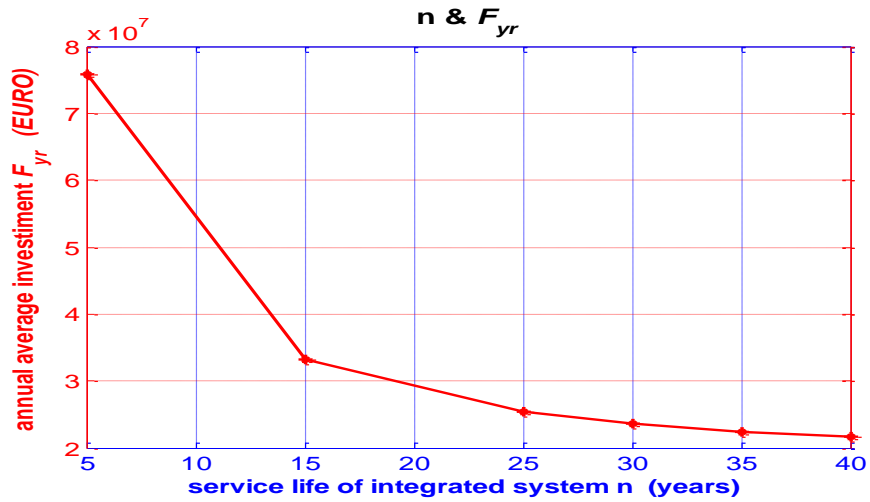


Figure 5.5: Variations of annual average investment Vs. service life.

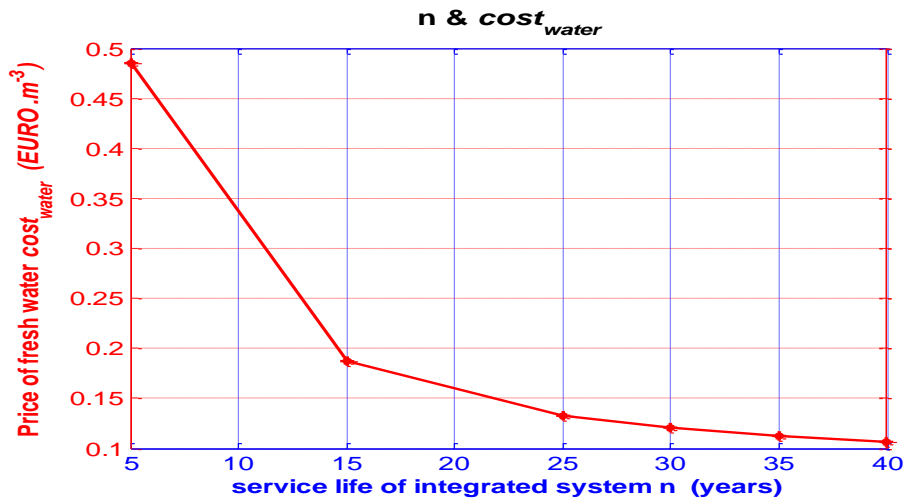


Figure 5.6: Variations of annual price of fresh water production Vs. service life.

5.5 Variations with Annual Interest Rate

The interest rate of CSCSPD used in this study was 6.2%. Figures 5.7 and 5.8 shows the results obtained from economic analysis. Figure 5.7 shows the variations of annual average investment Vs. annual interest rate. Figure 5.8 shows the price of freshwater Vs. annual interest rate. From Fig 5.7 it can be seen that the annual average investment cost of fresh water varies linearly with annual interest rate. From Fig 5.8. it can be seen that the cost of fresh water varies linearly with annual interest rate.

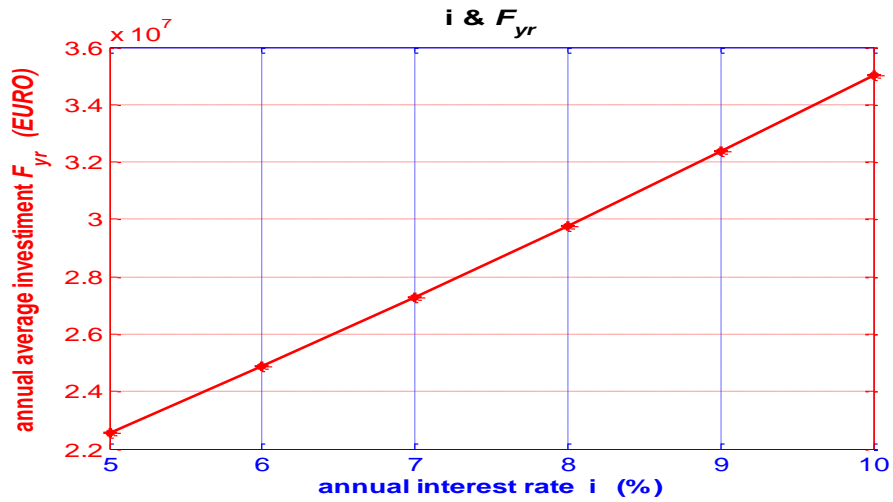


Figure 5.7: Variations of annual average investment Vs. annual interest rate.

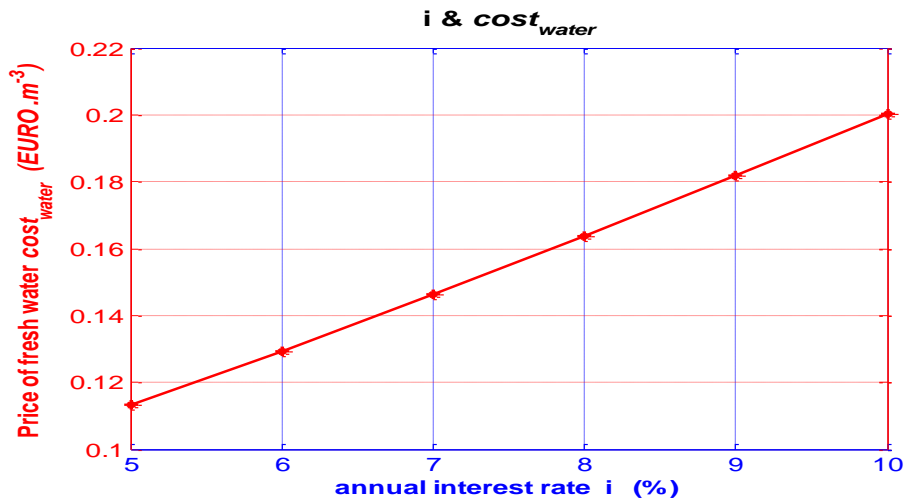


Figure 5.8: Variations of annual price of fresh water production Vs. annual interest rate.

5.6 Variations with MFR of Condensed Vapor in the Chimney and in the HEC

Both of the MFR of condensed vapor in the chimney and in the HEC represent the fresh water production. The increment in annual production for freshwater was the driving force in reducing the annual cost of fresh water production. Figure 5.9 shows the cost of fresh water Vs. MFR of total condensed water. It is clear that as the fresh water production increased the cost decreased.

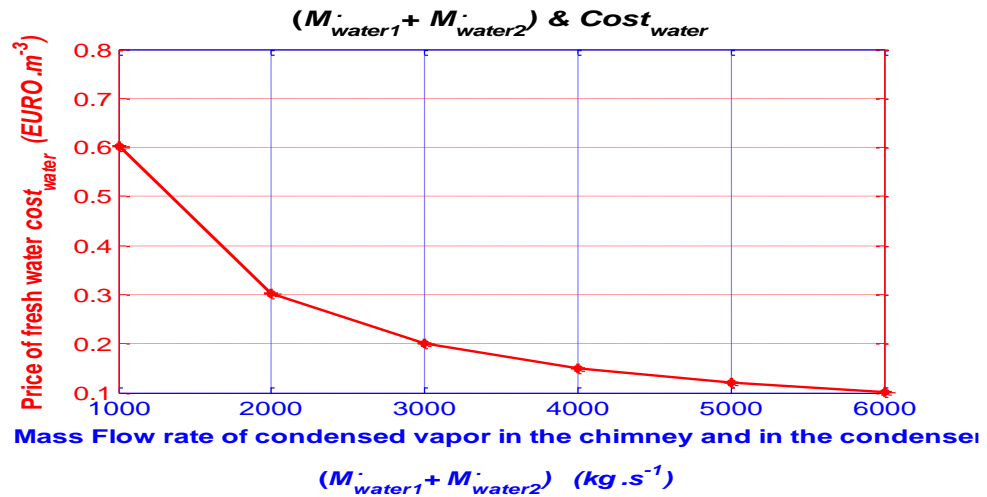


Figure 5.9: Variations of annual price of fresh water production Vs. MFR of vapor that condensed both in chimney and in condenser.

5.7 Variations with Running Hours

If the operation period time of the CSCSPD is taken for different hours every day [2] [4], the estimated results vary.

Table 5.1 shows the yearly power output, the yearly electricity revenue, the yearly CO₂ emission reduction, the yearly CO₂ revenue, the yearly fresh water production, the price of fresh water for different operating hours.

Table 5.1: Comparison of economic performance of the CSCSPD system with different operation periods (hours).

Parameters	Running hours during a days					
	5	6	7	8	9	24
Power output, kWh/year	$4.1158 \cdot 10^6$	$4.938 \cdot 10^6$	$5.76 \cdot 10^6$	$6.584 \cdot 10^6$	$7.407 \cdot 10^6$	$1.975 \cdot 10^7$
Electricity revenue, €/year	$1.234 \cdot 10^6$	$1.481 \cdot 10^6$	$1.728 \cdot 10^6$	$1.975 \cdot 10^6$	$2.222 \cdot 10^6$	$5.925 \cdot 10^6$
CO ₂ emission reduction, ton/year	$3.909 \cdot 10^6$	$4.691 \cdot 10^6$	$5.473 \cdot 10^6$	$6.255 \cdot 10^6$	$7.036 \cdot 10^6$	$1.876 \cdot 10^7$
CO ₂ revenue, €/year	$8.365 \cdot 10^7$	$1.004 \cdot 10^8$	$1.171 \cdot 10^8$	$1.338 \cdot 10^8$	$1.506 \cdot 10^8$	$4.015 \cdot 10^8$
Fresh water productivity, ton/year	$2.983 \cdot 10^7$	$3.58 \cdot 10^7$	$4.176 \cdot 10^7$	$4.773 \cdot 10^7$	$5.369 \cdot 10^7$	$1.432 \cdot 10^8$
Fresh water price, €/m ³	0.6371	0.5309	0.4551	0.3982	0.354	0.1327

The estimated results are compared with the results presented in Table 5.2 [2]. The price of freshwater extracted by the CSCSPD system is within to the range or to the price limit for the price of freshwater produced by systems running on conventional energy and wind energy systems. If the system is installed in an area exposed to solar power for a long time and to high solar radiation, the fresh water extracted from this system has the ability to compete in the local market.

According to the quantities and the price of electric power and fresh water produced from the plant, the payback period value is less than 13 years.

Table 5.2: The unit price of freshwater that works with multiple sources energies [2].

The energy	(price/m³)
Solar collectors	3.50€-8.00€
Photovoltaic	3.14€-9.00€
Wind	1.00€-5.00€
Conventional	0.35€-2.70€

Chapter 6

CONCLUSION

6.1 Mathematical and Economic Conclusions

The CSCSPD system is based on a set of new principles that operate simultaneously for the production of fresh water and electrical energy. In order to obtain the optimum capacity, a mathematical and economic model have been developed. Furthermore, alterations are possible within the large number of variables in the system to facilitate solutions for it to work at the highest performance level possible. The following conclusions were obtained for the CSCSPD system based on a mathematical and economic analysis.

1- This system has the ability to produce electrical energy and seawater desalination at the same time so it is considered a multi-output production system.

2- According to the results of the parameter's variations estimated by programmed mathematical method, the performance of CSCSPD increases with most of the parameters.

3- This system is installed on unused, vacant land near the sea and so it is of great significance in increasing the efficiency of the use of this land. This system is open to many technologies that are related to solar energy: evaporation, condensation and seawater desalination. Additionally, the HEC is considered as a heat exchanger. The

CSCSPD system and SSCS use the same land area but fresh water production is what makes the use of the first system better than the second system.

4- The economic results that have been obtained from the implementation of the economic model for the CSCSPD system are based on the price of electric power and the price of seawater desalination in Dalian, China.

6.2 Ecological and Social Conclusions

1- Through the creation of these systems, the power and clean water supply will increase in those areas affected and will be of special benefit to populated areas previously denied the benefits.

2- This system does not need direct sunlight and can operate successfully in weather conditions that receive only diffused or reflected sunlight because of partially or fully clouded skies.

3- Wind energy is considered intermittent, so the dependence on this type of system (CSCSPD) attracts development for short and long term development.

4- The construction of such a system is relatively simple because the required materials for the construction process are readily available. The construction technology is widely known, and the operating and maintenance costs are at the lowest possible levels.

5- The benefits of the CSCSPD system are that it only uses arable land, it does not have any negative impact on the environment, it does not destroy natural resources, does not cause migration problems for human beings or for animals, it operates only

using vacant land, it improves the environment, reduces the problem of water shortage and increases the agricultural production rate.

6- If it is possible to implement this solar system in an empty region, it will provide returns with huge benefits socially, economically and agriculturally.

6.3 Future Challenges

As presented in this thesis, many interesting properties and parameters of the CSCSPD have been detailed. This is particularly exceptional and encouraging given the relatively short period of CSCSPD research. By reviewing the results estimated from our programmed mathematical technique, we conclude that:

1- The limited research on CSCSPD is a result of the short period given to put plants of this kind in working order, the number of sites that have been installed, the results derived from experiments or theoretical studies, the presence of such projects and the high price required to set up such projects. However, this field is still open for more extended research, experiments, theoretical and economic analysis.

2- Although the condenser is one of the most important parts in CSCSPD studies, research at a theoretical and experimental level on the effectiveness of the condenser has been very limited.

3- The characteristics of CSCSPD complement and are well suited to Northern Cyprus' climatic conditions, in terms of its annual sunshine average as well as its geological, ecological, social economic conditions. It would also satisfy the need to reduce the consumption of conventional energy sources.

Finally, the implementation of a CSCSPD system greatly opens up the prospects of the benefits of solar energy and its applications, especially those systems producing electrical energy and freshwater from seawater desalination as multi-production systems.

REFERENCES

- [1] E.Delyannis, "Historic Background of Desalination and Renewable Energies," *Solar Energy*, vol. 75, pp. 357-366, 2003.
- [2] L. Zou, Y. Zheng, Z. Li and Y. Sha, "Solar Chimneys Integrated with Seawater Desalination," *Desalination*, vol. 276, pp. 207-213, 2011.
- [3] J. P. Pretorius and D. G. Kroger, "Critical Evaluation of Solar Chimney Power Plant Performance," *Solar Energy*, vol. 80, pp. 535-544, 2006.
- [4] X. P. Zhou, B. Xiao, W. C. Liu, X. J. Guo, J. K. Yang and J. Fan, "Comparison of Classical Solar Chimney Power System and Combined Solar Chimney System for Power Generation and Seawater Desalination," *Desalination*, vol. 250, pp. 249-256, 2010.
- [5] Y. P. Wang, Z. L. Fang, L. Zhu, Z. Y. Yang, J. H. Wang and L. J. Han, "Study on The Integrated Utilization of Seawater by Solar Chimney," *Acta Energy*, vol. 27, pp. 382-387, 2006.
- [6] L. Zou, Y. Yuan, Z. Li and Y. Zheng, "Experimental Research on Solar Chimneys Integrated with Seawater Desalination under Practical Weather Condition," *Desalination*, vol. 298, pp. 22-33, 2012.

- [7] J. Schlaich, *The Solar Chimney: Electricity from The Sun*, Stuttgart, Germany: Edition Axel Menges, 1995.
- [8] R. Robert, "Spanish Solar Chimney near Completion," *MPS Review*, vol. 6, pp. 21-23, 1981.
- [9] W. Haaf, k. Friedrich, G. Mayer and J. Schlaich, "Solar Chimneys Part I: Principle and Construction of The Pilot Plant in Manzanares," *International Journal of Solar Energy*, vol. 2, pp. 3-20, 1983.
- [10] W. Haaf, "Part II: Preliminary Test Results from The Manzanares Pilot Plant," *International Journal of Solar Energy*, vol. 2, pp. 141-161, 1984.
- [11] S. Terol, "The Present State of Research at The Solar Chimney Power Plant in Manzanares (Spain) and Future Prospects for Large Scale Plants," *International Congress on Renewable Energy Sources*, vol. 1, p. 1644, 1987.
- [12] M. A. d. S. Bernardes, "Solar Chimney Power Plants—Developments and Advancements," *Solar Energy*, pp. 978-953, 2010.
- [13] R. Daba, "Modeling and Simulation of Solar Chimney Power Plant with and without The Effect of Thermal Energy Storage Systems," *MSME*, 2011.

- [14] J. Pretorius, "Optimization and Control of a Large-scale Solar Chimney power plant," *Ph.D. dissertation*, available at:
http://www.crses.sun.ac.za/files/research/completed-research/solar/jp_pretorius.pdf, 2007.
- [15] X. S. Ge and H. Ye, "Solar Chimney Electric Generation System and Analysis of its Intrinsic Thermodynamic Defect," *Acta Energy*, vol. 25, pp. 263-268, 2004.
- [16] P. I. Cooper, "Digital Simulation of Transient Solar Still Processes," *Solar Energy*, vol. 12, pp. 313-325, 1969.
- [17] L. Zuo, Y. Yuan, Z. Li and W. Liu, "The Influence of Heat Collector Structural Parameters on The Solar Chimneys Integrated with Seawater Desalination," *International Conference on Sustainable Power Generation and Supply*, Hangzhou, China (8-9 Sept), 2012 .
- [18] L. Zuo, Y. Yuan, Z. Li and W. Liu, "Numerical Analysis of Flow Heat Transfer Characteristics in Solar Chimneys Integrated," *International Conference on Sustainable Power Generation and Supply*, Hangzhou, China (8-9 Sept), 2012 .
- [19] J. h. Wang, N. y. Gao, Y. Deng and Y. l. Li, "Solar Power-Driven Humidification-Dehumidification (HDH) Process for Desalination of Brackish Water," *Desalination*, vol. 305, pp. 17-23, 2012.

- [20] T. W. von Backstrom and A. J. Gannon, "Compressible Flow through Solar Power Plant Chimneys," *Solar Energy Engineering* , vol. 122, pp. 138-145, 2000.
- [21] Y. A. Cengel, heat transfer : a practical approach, new york: mcgraw-hill companies, 2014.
- [22] X. Zhou, J. Yang, B. Xiao, G. Hou and F. Xing, "Analysis of Chimney Height for Solar Chimney Power Plant," *Thermal Energy* , 2008.
- [23] R. Hardy, "ITS-90 Formulations for Vapor Pressure, Frostpoint Temperature, Dewpoint Temperature and Enhancement Factors in The Range -100," in *The Third International Symposium on Humidity and Moisture*, London , 1998 .
- [24] X. P. Zhou, J. K. Yang, R. M. Ochieng and B. Xiao, "Numerical Investigation Solar Chimney of A Plume from A Power Generation Solar Chimney in An Atmospheric Cross Flow," *Atmospheric Research*, vol. 91, pp. 26-35, 2009.
- [25] "The Engineering Toolbox," [Online]. Available:
<http://www.engineeringtoolbox.com>.
- [26] W. S. James and S. R. Parsons, "The Effect of Altitude on Radiator Performance," NACA Annual Report 5, United States, 1920.

- [27] “world weather and climate information,” [Online]. Available:
<http://www.weather-and-climate.com/average-monthly-Rainfall-Temperature-Sunshine,Dalian,China>.
- [28] A. Dhahri and A. Omri, “A Review of Solar Chimney Power Generation Technology,” *International Journal of Engineering and Advanced Technology*, vol. 2, no. 3, pp. 1-17, 2013.
- [29] J. y. Li, P. h. Guo and Y. Wang, “Effects of Collector Radius and Chimney Height on Power Output of A Solar Chimney Power Plant with Turbines,” *School of Energy and Power Engineering, Xian University*, 2012.
- [30] “Geometric Altitude vs. Temperature, Pressure, Density and The Speed of Sound,” *Standard Atmosphere, United States*, 1962.
- [31] Parida, Bhubaneswari, S. Iniyani and R. Goic, “A Review of Solar Photovoltaic Technologies,” *Renewable and Sustainable Energy Reviews*, vol. 15.3, pp. 1625-1636, 2011.
- [32] X. P. Zhou, J. K. Yang, F. Wang and B. Xiao, “Economic Analysis of Floating Solar Chimney Power Plant,” *Renewable and Sustainable Energy Reviews*, vol. 13, pp. 736-749, 2009.

[33] T. P. Fluri, J. P. Pretorius, C. P. van Dyk, T. W. van Backstrom, G. P. A. G. van Zijl and D. G. Kroger, "Cost Analysis Of Solar Chimney Power Plant," in *Proceedings of EuroSun*, Glasgow, Scotland, 2006.

[34] D. L. Talavera, G. Nofuentes, J. Aguilera and M. Fuentis, "Tables for The Estimation of The Internal Rate of Return of Photovoltaic Grid-Connected Systems," *Renewable and Sustainable Energy Reviews*, vol. 11, pp. 447-466, 2007.

APPENDICES

Appendix 1: The code of MATLAB for mathematical model

```
1. format short
2. close all;
3. clc;
4. % % *****Graph1*****
5. Rcoll=2000:500:4500;
6. Acoll=pi*((Rcoll-80).^2);
7. Upp=0.38;
8. s=1000;
9. ptotal=Upp*Acoll*s;
10. figure();
11. plot(Rcoll,ptotal,'*-r','linewidth',2);
12. xlabel('Collector radius \itR_{coll}
(m)','fontsize',12,'fontweight','b','color','b');
13. ylabel('Power output \itW^{.}_{total}
(W)','fontsize',12,'fontweight','b','color','r');
14. title('\itR_{coll} & \itW^{.}_{total}','fontsize',13,'fontweight','b','color','k');
15. set(gca,'Xcolor','b','Ycolor','r','fontsize',12);
16. grid on;
17. % % *****Graph2*****
18. Rcoll=2000:500:4500;
19. Acoll=pi*((Rcoll-80).^2);
20. ptotal=10315355980;
21. s=1000;
22. Upp=ptotal./(Acoll*s);
23. Upp=Upp*100;
24. figure();
25. plot(Rcoll,Upp,'*-r','linewidth',2);
26. xlabel('Collector radius \itR_{coll}
(m)','fontsize',12,'fontweight','b','color','b');
27. ylabel('Efficiency \eta\it_{\rho\rho}
(%)','fontsize',12,'fontweight','b','color','r');
28. title('\itR_{coll} & \eta\it_{\rho\rho}','fontsize',13,'fontweight','b','color','k');
29. set(gca,'Xcolor','b','Ycolor','r','fontsize',12);
30. grid on;
31. % % *****Graph3*****
32. s=500:200:1200;
33. Upp=0.38;
34. Acoll=26786475.601;
35. ptotal=Upp*Acoll*s;
36. figure();
37. plot(s,ptotal,'*-r','linewidth',2);
38. xlabel('Solar Radiation I (W\it.m^{-2})','fontsize',12,'fontweight','b','color','b');
39. ylabel('Power output \itW^{.}_{total}
(w)','fontsize',12,'fontweight','b','color','r');
40. title('I & \itW^{.}_{total}','fontsize',13,'fontweight','b','color','k');
41. set(gca,'Xcolor','b','Ycolor','r','fontsize',12);
```

```

42. grid on;
43. % % *****Graph4*****
44. clear all;
45. Acoll=26786475.601;
46. ptotal=10261242980;
47. s=500:500:3000;
48. Upp=ptotal./(Acoll*s);
49. Upp=Upp*100;
50. figure();
51. plot(s,Upp,'*-r','linewidth',2);
52. xlabel('Solar Radiation I ( $W/m^2$ )','fontsize',12,'fontweight','b','color','b');
53. ylabel('Efficiency  $\eta_{\rho}$ '
    (%)','fontsize',12,'fontweight','b','color','r');
54. title('I &  $\eta_{\rho}$ ','fontsize',13,'fontweight','b','color','k');
55. set(gca,'Xcolor','b','Ycolor','r','fontsize',12);
56. grid on;
57. % *****Graph5*****
58. clear all;
59. Acoll=26786475.601;
60. ptotal=0:50:250;
61. s=1000;
62. Upp=ptotal./(Acoll*s);
63. Upp=Upp*1e8;
64. figure();
65. plot(ptotal,Upp,'*-r','linewidth',2);
66. xlabel('Power output  $W_{total}$ '
    (W)','fontsize',12,'fontweight','b','color','b');
67. ylabel('Efficiency  $\eta_{\rho}$ '
    (%)','fontsize',12,'fontweight','b','color','r');
68. title('\mathit{W}^{.}_{total} &
    \eta_{\rho}','fontsize',13,'fontweight','b','color','k');
69. set(gca,'Xcolor','b','Ycolor','r','fontsize',12);
70. grid on;
71. % % % % *****Graph6*****
72. clear all;
73. Dmwater2=0:1000:5000;
74. Mwg=0.9;
75. g=9.81;
76. H1=500;
77. Pwg=Mwg*Dmwater2*g*H1;
78. Pat=39200000;
79. ptotal=Pat+Pwg;
80. figure();
81. plot(Dmwater2,ptotal,'*-r','linewidth',2);
82. xlabel('Mass Flow rate of condenser vapor in the condenser  $M_{water2}$ '
    (Kg.s-1)','fontsize',12,'fontweight','b','color','b');
83. ylabel('Power output  $W_{total}$ '
    (W)','fontsize',12,'fontweight','b','color','r');
84. title('\mathit{M}^{.}_{water2} & \mathit{W}^{.}_{total}'
    ','fontsize',13,'fontweight','b','color','k');

```

```

85. set(gca,'Xcolor','b','Ycolor','r','fontsize',12);
86. grid on;
87. % *****Graph7*****
88. clear all;
89. Dmwater2=0:1000:5000;
90. Mwg=0.9;
91. g=9.81;
92. H1=500;
93. Pwg=Mwg*Dmwater2*g*H1;
94. Pat=39200000;
95. hf=2260000*Dmwater2;
96. ptotal=Pat+Pwg+hf;
97. Acoll=26786475.601;
98. s=1000;
99. Upp=ptotal./(Acoll*s);
100. Upp=Upp*100;
101. figure();
102. plot(Dmwater2,Upp,'*-r','linewidth',2);
103. xlabel('Mass Flow rate of condenser vaper in the condenser \itM^{\rho}
        \it_{water2} \it(Kg.s^{-1}) ','fontsize',12,'fontweight','b','color','b');
104. ylabel('Efficiency \eta\it_{\rho\rho} (%)','fontsize',12,'fontweight','b','color','r');
105. title('\itM^{\rho} \it_{water2} & \eta\it_{\rho\rho} ','fontsize',13,'fontweight','b','color','k');
106. set(gca,'Xcolor','b','Ycolor','r','fontsize',12);
107. grid on;
108. % *****Graph8*****
109. clear all;
110. Dmwater2=3378.223;
111. Mwg=0.9;
112. g=9.81;
113. H1=300:200:1300;
114. Pwg=Mwg*Dmwater2*g*H1;
115. Pat=39200000;
116. ptotal=Pat+Pwg;
117. figure();
118. plot(H1,ptotal,'*-r','linewidth',2);
119. xlabel('Chimney hieght \itH_1 (m) ','fontsize',12,'fontweight','b','color','b');
120. ylabel('Power output \itW^{\rho} \it_{total} (W)','fontsize',12,'fontweight','b','color','r');
121. title('\itH_1 & \itW^{\rho} \it_{total} ','fontsize',13,'fontweight','b','color','k');
122. set(gca,'Xcolor','b','Ycolor','r','fontsize',12);
123. grid on;
124. axis([300 1300 4.5*10^7 8*10^7]);

125. % *****Graph9*****
126. clear all;
127. Dmwater2=3378.223;
128. Mwg=0.9;

```

```

129. g=9.81;
130. H1=300:200:1300;
131. Pwg=Mwg*Dmwater2*g*H1;
132. Pat=10300442980;
133. ptotal=Pat+Pwg;
134. Acoll=26786475.601;
135. s=1000;
136. Upp=ptotal./(Acoll*s);
137. Upp=Upp*100;
138. figure();
139. plot(H1,Upp,'*-r','linewidth',2);
140. xlabel('Chimney hieght \itH_1
(m)','fontsize',12,'fontweight','b','color','b');
141. ylabel('Efficiency \eta\it_{\rho\rho}
(%)','fontsize',12,'fontweight','b','color','r');
142. title('\itH_1 & \eta\it_{\rho\rho} ','fontsize',13,'fontweight','b','color','k');
143. set(gca,'Xcolor','b','Ycolor','r','fontsize',12);
144. grid on;
145. % *****Graph10*****
146. clear all;
147. r=20:20:120;
148. Ach=pi*r.^2;
149. jat=0.8; n=0.9;M1=7.58; Dp=357.23;
150. Pat=jat*n*Ach*M1*Dp;
151. Pwg=14913196.335;
152. ptotal=Pat+Pwg;
153. figure();
154. plot(r,ptotal,'*-r','linewidth',2);
155. xlabel('Chimney radius r (m) ','fontsize',12,'fontweight','b','color','b');
156. ylabel('Power output \itW^{\cdot}_{total}
(W)','fontsize',12,'fontweight','b','color','r');
157. title('r & \itW^{\cdot}_{total} ','fontsize',13,'fontweight','b','color','k');
158. set(gca,'Xcolor','b','Ycolor','r','fontsize',12);
159. grid on;
160. % *****Graph11*****
161. clear all;
162. r=20:20:120;
163. Ach=pi*r.^2;
164. jat=0.8; n=0.9;M1=7.58; Dp=357.23;
165. Pat=jat*n*Ach*M1*Dp;
166. Pwg=10276156176.335;
167. ptotal=Pat+Pwg;
168. Acoll=26786475.601;
169. s=1000;
170. Upp=ptotal./(Acoll*s);
171. Upp=Upp*100;
172. figure();
173. plot(r,Upp,'*-r','linewidth',2);
174. xlabel('Chimney radius r (m) ','fontsize',12,'fontweight','b','color','b');

```

```

175. ylabel('Efficiency \eta\it_{\rho\rho}
      (%)','fontsize',12,'fontweight','b','color','r');
176. title('r & \eta\it_{\rho\rho} ','fontsize',13,'fontweight','b','color','k');
177. set(gca,'Xcolor','b','Ycolor','r','fontsize',12);
178. grid on;
179. % *****Graph12*****
180. clear all;
181. Ach=20106.192;
182. jat=0.8; n=0.9;M1=7.58;
183. Dp=100:100:800;
184. Pat=jat*n*Ach*M1*Dp;
185. Pwg=14913196.335;
186. ptotal=Pat+Pwg;
187. figure();
188. plot(Dp,ptotal,'*-r','linewidth',2);
189. xlabel('The pressure difference \Delta P
      (Pa)','fontsize',12,'fontweight','b','color','b');
190. ylabel('Power output \itW^{\cdot}_{total}
      (W)','fontsize',12,'fontweight','b','color','r');
191. title('\Delta P & \itW^{\cdot}_{total} ','fontsize',13,'fontweight','b','color','k');
192. set(gca,'Xcolor','b','Ycolor','r','fontsize',12);
193. grid on;
194. % *****Graph13*****
195. clear all;
196. Ach=20106.192;
197. jat=0.8; n=0.9;M1=7.58;
198. Dp=100:100:800;
199. Pat=jat*n*Ach*M1*Dp;
200. Pwg=10276156176.335;
201. ptotal=Pat+Pwg;
202. Acoll=26786475.601;
203. s=1000;
204. Upp=ptotal./(Acoll*s);
205. Upp=Upp*100;
206. figure();
207. plot(Dp,Upp,'*-r','linewidth',2);
208. xlabel('The pressure difference \Delta P (Pa)
      ','fontsize',12,'fontweight','b','color','b');
209. ylabel('Efficiency \eta\it_{\rho\rho}
      (%)','fontsize',12,'fontweight','b','color','r');
210. title('\Delta P & \eta\it_{\rho\rho} ','fontsize',13,'fontweight','b','color','k');
211. set(gca,'Xcolor','b','Ycolor','r','fontsize',12);
212. grid on;
213. % *****Graph14*****
214. clear all;
215. Ach=20106.192;
216. jat=0.8; n=0.9; Dp=357.23;
217. M1=2:2:12;
218. Pat=jat*n*Ach*M1*Dp;
219. Pwg=14913196.335;

```



```

220. ptotal=Pat+Pwg;
221. figure();
222. plot(M1,ptotal,'*-r','linewidth',2);
223. xlabel('The Velocity of air flow at chimney intel U\it_1 (m\it.s^{\-
1}),'fontsize',12,'fontweight','b','color','b');
224. ylabel('Power output \itW^{\cdot}_{total}
(W)'fontsize',12,'fontweight','b','color','r');
225. title('U\it_1 & \itW^{\cdot}_{total} ',fontsize',13,'fontweight','b','color','k');
226. set(gca,'Xcolor','b','Ycolor','r','fontsize',12);
227. grid on;
228. % *****Graph15*****
229. clear all;
230. Ach=20106.192;
231. jat=0.8; n=0.9; Dp=357.23;
232. M1=2:2:12;
233. Pat=jat*n*Ach*M1*Dp;
234. Pwg=10276156176.335;
235. ptotal=Pat+Pwg;
236. Acoll=26786475.601;
237. s=1000;
238. Upp=ptotal./(Acoll*s);
239. Upp=Upp*100;
240. figure();
241. plot(M1,Upp,'*-r','linewidth',2);
242. xlabel('The Velocity of air flow at chimney intel U\it_1 (m\it.s^{\-
1}),'fontsize',12,'fontweight','b','color','b');
243. ylabel('Efficiency \eta\it_{\rho\rho}
(%)'fontsize',12,'fontweight','b','color','r');
244. title('U\it_1 & \eta\it_{\rho\rho} ',fontsize',13,'fontweight','b','color','k');
245. set(gca,'Xcolor','b','Ycolor','r','fontsize',12);
246. grid on;
247. % % *****Graph16*****
248. clear all;
249. E=0:0.2:1;
250. Qmax=2750152.707;
251. Q=E*Qmax;
252. T2=34.7;
253. CR2=176156.059;
254. T3=((CR2*T2)-Q)/CR2;
255. p3=94545;
256. pv3=[5.5432e+03 4.6514e+03 3.8887e+03 3.2378e+03 2.6811e+03
2.2140e+03];
257. d3=0.62198*(pv3./(p3-pv3));
258. Mf2=162805.97;
259. d2=0.0383;
260. DMwater2=Mf2*((d2/(1+d2))-(d3/(1+d3)));
261. Mwg=0.9; g=9.81; H1=500;
262. pwg=Mwg*DMwater2*g*H1;
263. pat=39200000;
264. ptotal=pat+pwg;

```

```

265. figure();
266. plot(E,ptotal,'*-r','linewidth',2);
267. xlabel('The Effectiveness of the condenser \epsilon (%)
', 'fontsize',12,'fontweight','b','color','b');
268. ylabel('Power output \itW^{\cdot} _{total}
(W)', 'fontsize',12,'fontweight','b','color','r');
269. title('\epsilon & \itW^{\cdot} _{total} ', 'fontsize',13,'fontweight','b','color','k');
270. set(gca,'Xcolor','b','Ycolor','r','fontsize',12);
271. grid on;
272. % *****Graph17*****
273. clear all;
274. E=0:0.2:1;
275. Qmax=2750152.707;
276. Q=E*Qmax;
277. T2=34.7;
278. CR2=176156.059;
279. T3=((CR2*T2)-Q)/CR2;
280. p3=94545;
281. pv3=[5.5432e+03 4.6514e+03 3.8887e+03 3.2378e+03 2.6811e+03
2.2140e+03];
282. d3=0.62198*(pv3./(p3-pv3));
283. Mf2=162805.97;
284. d2=0.0383;
285. DMwater2=Mf2*((d2/(1+d2))-(d3/(1+d3)));
286. Mwg=0.9; g=9.81; H1=500;
287. pwg=Mwg*DMwater2*g*H1;
288. pat=39200000;
289. ptotal=pat+pwg+10261242980;
290. Acoll=26786475.601;
291. s=1000;
292. Upp=ptotal./(Acoll*s);
293. Upp=Upp*100;
294. figure();
295. plot(E,Upp,'*-r','linewidth',2);
296. xlabel('The Effectiveness of the condenser \epsilon (%)
', 'fontsize',12,'fontweight','b','color','b');
297. ylabel('Efficiency \eta_{\rho\rho}
(%)', 'fontsize',12,'fontweight','b','color','r');
298. title('\epsilon & \eta_{\rho\rho} ', 'fontsize',13,'fontweight','b','color','k');
299. set(gca,'Xcolor','b','Ycolor','r','fontsize',12);
300. grid on;
301. % *****Graph18*****
302. figure();
303. plot(E,DMwater2,'*-r','linewidth',2);
304. str={'Mass flow rate of condensed vapor in ', ...
305. };
306. xlabel('The Effectiveness of the condenser \epsilon (%)
', 'fontsize',12,'fontweight','b','color','b');
307. ylabel([str, 'the condenser \itM^{\cdot} _{water2} \it(Kg.s^{\cdot}
1)']), 'fontsize',12,'fontweight','b','color','r');

```

```

308. title('\epsilon & \itM^{.}\it_{water2}
      ', 'fontsize', 13, 'fontweight', 'b', 'color', 'k');
309. set(gca, 'Xcolor', 'b', 'Ycolor', 'r', 'fontsize', 12);
310. grid on;
311. % *****Graph19*****
312. clear all;
313. Ma=50000:50000:250000;
314. Cpa1=1.0271;
315. CRa=Ma*Cpa1;
316. DTmax=22.95;
317. E=0.9;
318. Qmax=CRa*DTmax;
319. Q=E*Qmax;
320. T2=34.7;
321. CR2=176156.059;
322. T3=((CR2*T2)-Q)/CR2;
323. p3=94545;
324. pv3=[ 3.9405e+03 2.7571e+03 1.8969e+03 1.2817e+03 849.5797 ];
325. d3=0.62198*(pv3./(p3-pv3));
326. Mf2=162805.97;
327. d2=0.0383;
328. DMwater2=Mf2*((d2/(1+d2))-(d3./(1+d3)));
329. Mwg=0.9; g=9.81; H1=500;
330. pwg=Mwg*DMwater2*g*H1;
331. pat=39200000;
332. ptotal=pat+pwg;
333. figure();
334. plot(Ma, ptotal, '-r', 'linewidth', 2);
335. set(gca, 'XTickLabel', Ma);
336. xlabel('Mass flow rate of ambient air M^{.}\it_a \it(kg.s^{-1})
      ', 'fontsize', 12, 'fontweight', 'b', 'color', 'b');
337. ylabel('Power output \itW^{.}\it_{total}
      (W)', 'fontsize', 12, 'fontweight', 'b', 'color', 'r');
338. title('\itM^{.}\it_a & \itW^{.}\it_{total}
      ', 'fontsize', 13, 'fontweight', 'b', 'color', 'k');
339. set(gca, 'Xcolor', 'b', 'Ycolor', 'r', 'fontsize', 12);
340. grid on;
341. % *****Graph20*****
342. clear all;
343. Ma=50000:50000:250000;
344. Cpa1=1.0271;
345. CRa=Ma*Cpa1;
346. DTmax=22.95;
347. E=0.9;
348. Qmax=CRa*DTmax;
349. Q=E*Qmax;
350. T2=34.7;
351. CR2=176156.059;
352. T3=((CR2*T2)-Q)/CR2;
353. p3=94545;

```

```

354. pv3=[ 3.9405e+03 2.7571e+03 1.8969e+03 1.2817e+03 849.5797 ];
355. d3=0.62198*(pv3./(p3-pv3));
356. Mf2=162805.97;
357. d2=0.0383;
358. DMwater2=Mf2*((d2/(1+d2))-(d3./(1+d3)));
359. Mwg=0.9; g=9.81; H1=500;
360. pwg=Mwg*DMwater2*g*H1;
361. pat=10300442980;
362. ptotal=pat+pwg;
363. Acoll=26786475.601;
364. s=1000;
365. Upp=ptotal./(Acoll*s);
366. Upp=Upp*100;
367. figure();
368. plot(Ma,Upp,'*-r','linewidth',2);
369. set(gca,'XTickLabel',Ma);
370. xlabel('Mass flow rate of ambient air M^{.}\it_a \it(kg.s^{-1})
', 'fontsize',12,'fontweight','b','color','b');
371. ylabel('Efficiency \eta\it_{\rho\rho}
(%)', 'fontsize',12,'fontweight','b','color','r');
372. title('\itM^{.}\it_a & \eta\it_{\rho\rho}
', 'fontsize',13,'fontweight','b','color','k');
373. set(gca,'Xcolor','b','Ycolor','r','fontsize',12);
374. grid on;
375. % % *****Graph21*****
376. clear all;
377. r=20:20:120;
378. Ach=pi*r.^2;
379. Acond=Ach;
380. Mug=5; Mg=123854.13;
381. pg=Mg./(Mug*Acond);
382. pa1=1.1608;
383. DF=pa1./pg;
384. Ma=Mg*DF;
385. Cpa1=1.0271;
386. CRa=Ma*Cpa1;
387. DTmax=22.95;
388. E=0.9;
389. Qmax=CRa*DTmax;
390. Q=E*Qmax;
391. T2=34.7;
392. CR2=176156.059;
393. T3=((CR2*T2)-Q)/CR2;
394. p3=94545;
395. pv3=[5.2748e+03 4.5512e+03 3.5305e+03 2.4381e+03 1.4754e+03
763.9779];
396. d3=0.62198*(pv3./(p3-pv3));
397. Mf2=162805.97;
398. d2=0.0383;
399. DMwater2=Mf2*((d2/(1+d2))-(d3./(1+d3)));

```

```

400. Mwg=0.9; g=9.81; H1=500;
401. pwg=Mwg*DMwater2*g*H1;
402. pat=39200000;
403. ptotal=pat+pwg;
404. figure();
405. plot(r,ptotal,'*-r','linewidth',2);
406. xlabel('Condenser radius \itR_{cond} (m)
         ','fontsize',12,'fontweight','b','color','b');
407. ylabel('Power output \itW^{.}_{total}
         (W)','fontsize',12,'fontweight','b','color','r');
408. title('\itR_{cond} & \itW^{.}_{total}
         ','fontsize',13,'fontweight','b','color','k');
409. set(gca,'Xcolor','b','Ycolor','r','fontsize',12);
410. grid on;
411. % *****Graph22*****
412. clear all;
413. r=20:20:120;
414. Ach=pi*r.^2;
415. Acond=Ach;
416. Mug=5; Mg=123854.13;
417. pg=Mg./(Mug*Acond);
418. pa1=1.1608;
419. DF=pa1./pg;
420. Ma=Mg*DF;
421. Cpa1=1.0271;
422. CRa=Ma*Cpa1;
423. DTmax=22.95;
424. E=0.9;
425. Qmax=CRa*DTmax;
426. Q=E*Qmax;
427. T2=34.7;
428. CR2=176156.059;
429. T3=((CR2*T2)-Q)/CR2;
430. p3=94545;
431. pv3=[5.2748e+03 4.5512e+03 3.5305e+03 2.4381e+03 1.4754e+03
         763.9779];
432. d3=0.62198*(pv3./(p3-pv3));
433. Mf2=162805.97;
434. d2=0.0383;
435. DMwater2=Mf2*((d2/(1+d2))-(d3./(1+d3)));
436. Mwg=0.9; g=9.81; H1=500;
437. pwg=Mwg*DMwater2*g*H1;
438. pat=1003004429;
439. ptotal=pat+pwg;
440. Acoll=26786475.601;
441. s=1000;
442. Upp=ptotal./(Acoll*s);
443. Upp=Upp*100;
444. figure();
445. plot(r,Upp,'*-r','linewidth',2);

```

```

446. xlabel('Condenser radius \itR_{cond} (m)
      ', 'fontsize', 12, 'fontweight', 'b', 'color', 'b');
447. ylabel('Efficiency \eta\it_{\rho\rho}
      (%)', 'fontsize', 12, 'fontweight', 'b', 'color', 'r');
448. title('\itR_{cond} & \eta\it_{\rho\rho}
      ', 'fontsize', 13, 'fontweight', 'b', 'color', 'k');
449. set(gca, 'Xcolor', 'b', 'Ycolor', 'r', 'fontsize', 12);
450. grid on;
451. % *****Graph23*****
452. clear all;
453. Mach2=0:0.01:0.05;
454. C2=365.0177;
455. Mu2=Mach2*C2;
456. p2=1.0564; A2=20106.19;
457. Mf2=p2*Mu2*A2;
458. Cp2=1.082;
459. CR2=Mf2*Cp2;
460. Q=2475137.43711;
461. T2=34.7;
462. T3=T2-(Q./CR2);
463. p3=94545;
464. pv3=[ -inf 886.2760 2.3320e+03 3.1493e+03 3.6413e+03 3.9684e+03
      ];
465. d3=0.62198*(pv3./(p3-pv3));
466. Mf2=162805.97;
467. d2=0.0383;
468. DMwater2=Mf2*((d2/(1+d2))-(d3./(1+d3)));
469. Mwg=0.9; g=9.81; H1=500;
470. pwg=Mwg*DMwater2*g*H1;
471. pat=39200000;
472. ptotal=pat+pwg;
473. figure();
474. plot(Mach2, ptotal, '*-r', 'linewidth', 2);
475. xlabel('Mach number \itMach_2 ', 'fontsize', 12, 'fontweight', 'b', 'color', 'b');
476. ylabel('Power output \itW^{\ . }_{total}
      (W)', 'fontsize', 12, 'fontweight', 'b', 'color', 'r');
477. title('\itMach_2 & \itW^{\ . }_{total}
      ', 'fontsize', 13, 'fontweight', 'b', 'color', 'k');
478. set(gca, 'Xcolor', 'b', 'Ycolor', 'r', 'fontsize', 12);
479. grid on;
480. % *****Graph24*****
481. clear all;
482. Mach2=0:0.01:0.05;
483. C2=365.0177;
484. Mu2=Mach2*C2;
485. p2=1.0564; A2=20106.19;
486. Mf2=p2*Mu2*A2;
487. Cp2=1.082;
488. CR2=Mf2*Cp2;
489. Q=2475137.43711;

```

```

490. T2=34.7;
491. T3=T2-(Q./CR2);
492. p3=94545;
493. pv3=[ -inf 886.2760 2.3320e+03 3.1493e+03 3.6413e+03 3.9684e+03
];
494. d3=0.62198*(pv3./(p3-pv3));
495. Mf2=162805.97;
496. d2=0.0383;
497. DMwater2=Mf2*((d2/(1+d2))-(d3./(1+d3)));
498. Mwg=0.9; g=9.81; H1=500;
499. pwg=Mwg*DMwater2*g*H1;
500. pat=10300442980;
501. ptotal=pat+pwg;
502. Acoll=26786475.601;
503. s=1000;
504. Upp=ptotal./(Acoll*s);
505. Upp=Upp*100;
506. figure();
507. plot(Mach2,Upp,'*-r','linewidth',2);
508. xlabel('Mach number \itMach_2 ','fontsize',12,'fontweight','b','color','b');
509. ylabel('Efficiency \eta\it_{\rho\rho}
(%)','fontsize',12,'fontweight','b','color','r');
510. title('\itMach_2 & \eta\it_{\rho\rho}
','fontsize',13,'fontweight','b','color','k');
511. set(gca,'Xcolor','b','Ycolor','r','fontsize',12);
512. grid on;
513. % % % % % % *****Graph25*****
514. clear all;
515. format long;
516. DQ=100:100:600;
517. r=80;Cp1=1096.292;g=9.81;H1=500;Mach1=0.02049;
518. syms M;
519. Mach2(1)=solve('0.5*M^2-
log(M)+((79)/1096.292^2)*100+((9.81*500)/(1096.292^2))+log(0.02049)-
0.5*(0.02049^2)');
520. Mach2(2)=solve('0.5*M^2-
log(M)+((79)/1096.292^2)*200+((9.81*500)/(1096.292^2))+log(0.02049)-
0.5*(0.02049^2)');
521. Mach2(3)=solve('0.5*M^2-
log(M)+((79)/1096.292^2)*300+((9.81*500)/(1096.292^2))+log(0.02049)-
0.5*(0.02049^2)');
522. Mach2(4)=solve('0.5*M^2-
log(M)+((79)/1096.292^2)*400+((9.81*500)/(1096.292^2))+log(0.02049)-
0.5*(0.02049^2)');
523. Mach2(5)=solve('0.5*M^2-
log(M)+((79)/1096.292^2)*500+((9.81*500)/(1096.292^2))+log(0.02049)-
0.5*(0.02049^2)');
524. Mach2(6)=solve('0.5*M^2-
log(M)+((79)/1096.292^2)*600+((9.81*500)/(1096.292^2))+log(0.02049)-
0.5*(0.02049^2)');

```

```

525. T02=34.767; k=1.4;
526. T2=T02./(1+(Mach2.^2)*(k-1)/2);
527. p2=95440;Rd=287;Rs=461;
528. Pv2=[5.280903107304593e3 5.10891379185023e3
4.9087949575708e3 4.670132e3 4.480855254716292e3
4.280842892904921e3];
529. rah2=((p2-Pv2)./(Rd*(T2+273.15)))+(Pv2./(Rs*(T2+273.15)));

530. rah1=1.10194;
531. Beta=(rah2-rah1)./H1;
532. Ba=-0.00014; raha1=1.1608;
533. DP=g*(((raha1-rah1)*H1)-((1/2)*(Ba-Beta)*H1^2));

534. pwg=14913196.335;
535. Jag=0.8; n=0.9; Ach=20106.192;U1=7.58;
536. pat=Jag*n*Ach*U1*DP;
537. ptotal=pat+pwg;
538. figure();
539. plot(DQ,ptotal,'*-r','linewidth',2);
540. xlabel('Latent heat of Evaporation at chimney outlet \Delta Q
(KJ.K\itg^{-1}) ','fontsize',12,'fontweight','b','color','b');
541. ylabel('Power output \itW^{.}_{total}
(W) ','fontsize',12,'fontweight','b','color','r');
542. title('\Delta Q & \itW^{.}_{total} ','fontsize',13,'fontweight','b','color','k');
543. set(gca,'Xcolor','b','Ycolor','r','fontsize',12);
544. grid on;
545. % % % % % % *****Graph26*****
546. clear all;
547. format long;
548. DQ=100:100:600;
549. r=80;Cp1=1096.292;g=9.81;H1=500;Mach1=0.02049;
550. syms M;
551. Mach2(1)=solve('0.5*M^2-
log(M)+(((79)/1096.292^2)*100)+((9.81*500)/(1096.292^2))+log(0.02049)-
0.5*(0.02049^2)');
552. Mach2(2)=solve('0.5*M^2-
log(M)+((79)/1096.292^2)*200+((9.81*500)/(1096.292^2))+log(0.02049)-
0.5*(0.02049^2)');
553. Mach2(3)=solve('0.5*M^2-
log(M)+((79)/1096.292^2)*300+((9.81*500)/(1096.292^2))+log(0.02049)-
0.5*(0.02049^2)');
554. Mach2(4)=solve('0.5*M^2-
log(M)+((79)/1096.292^2)*400+((9.81*500)/(1096.292^2))+log(0.02049)-
0.5*(0.02049^2)');
555. Mach2(5)=solve('0.5*M^2-
log(M)+((79)/1096.292^2)*500+((9.81*500)/(1096.292^2))+log(0.02049)-
0.5*(0.02049^2)');

```



```

556. Mach2(6)=solve('0.5*M^2-
log(M)+((79)/1096.292^2)*600+((9.81*500)/(1096.292^2))+log(0.02049)-
0.5*(0.02049^2)');

557. T02=34.767; k=1.4;
558. T2=T02./(1+(Mach2.^2)*(k-1)/2);
559. p2=95440;Rd=287;Rs=461;
560. Pv2=[5.280903107304593e3 5.10891379185023e3
4.9087949575708e3 4.670132e3 4.480855254716292e3
4.280842892904921e3];
561. rah2=((p2-Pv2)./(Rd*(T2+273.15)))+(Pv2./(Rs*(T2+273.15)));

562. rah1=1.10194;
563. Beta=(rah2-rah1)./H1;
564. Ba=-0.00014; raha1=1.1608;
565. DP=g*(((raha1-rah1)*H1)-((1/2)*(Ba-Beta)*H1^2));

566. pwg=10276156176.335;
567. Jag=0.8; n=0.9; Ach=20106.192;U1=7.58;
568. pat=Jag*n*Ach*U1*DP;
569. ptotal=pat+pwg;
570. Acoll=26786475.601;
571. s=1000;
572. Upp=ptotal./(Acoll*s);
573. Upp=Upp*100;
574. figure();
575. plot(DQ,Upp,'*-r','linewidth',2);
576. xlabel('Latent heat of Evaporation at chimney outlet \Delta Q
(KJ.K\itg^{-1}) ','fontsize',12,'fontweight','b','color','b');
577. ylabel('Efficiency \eta\it_{\rho\rho}
(%),'fontsize',12,'fontweight','b','color','r');
578. title('\Delta Q & \eta\it_{\rho\rho} ','fontsize',13,'fontweight','b','color','k');
579. set(gca,'Xcolor','b','Ycolor','r','fontsize',12);
580. grid on;
581. % % % % % *****Graph27*****
582. clear all;
583. format long;
584. d2=0.0383;
585. d3=0.0164;
586. Mf2=[50000:50000:250000];
587. DMwater2=Mf2*((d2/(1+d2))-(d3/(1+d3)));
588. Mwg=0.9; g=9.81; H1=500;
589. pwg=Mwg*DMwater2*g*H1;
590. pat=39200000;
591. ptotal=pat+pwg;
592. figure();
593. plot(Mf2,ptotal,'*-r','linewidth',2);
594. set(gca,'XTickLabel',Mf2);
595. xlabel('Mass flow rate of operating air at chimney outlet \itM_{f2}
\it(kg.s^{-1}) ','fontsize',12,'fontweight','b','color','b');

```

```

596. ylabel('Power output \itW^{\ }_{total}
(W)', 'fontsize', 12, 'fontweight', 'b', 'color', 'r');
597. title('\itM^{\ }_{f2} & \itW^{\ }_{total}
', 'fontsize', 13, 'fontweight', 'b', 'color', 'k');
598. set(gca, 'Xcolor', 'b', 'Ycolor', 'r', 'fontsize', 12);
599. grid on;
600. % % % % % % % *****Graph28*****
601. clear all;
602. format long;
603. d2=0.0383;
604. d3=0.0164;
605. Mf2=[50000:50000:250000];
606. DMwater2=Mf2*((d2/(1+d2))-(d3/(1+d3)));
607. Mwg=0.9; g=9.81; H1=500;
608. pwg=Mwg*DMwater2*g*H1;
609. pat=10300442980;
610. ptotal=pat+pwg;
611. Acoll=26786475.601;
612. s=1000;
613. Upp=ptotal./(Acoll*s);
614. Upp=Upp*100;
615. figure();
616. plot(Mf2,Upp, '*-r', 'linewidth', 2);
617. set(gca, 'XTickLabel', Mf2);
618. xlabel('Mass flow rate of operating air at chimney outlet \itM_{f2}
\it(kg.s^{-1}) ', 'fontsize', 12, 'fontweight', 'b', 'color', 'b');
619. ylabel('Efficiency \eta\it_{\rho\rho}
(%)', 'fontsize', 12, 'fontweight', 'b', 'color', 'r');
620. title('\itM^{\ }_{f2} & \eta\it_{\rho\rho}
', 'fontsize', 13, 'fontweight', 'b', 'color', 'k');
621. set(gca, 'Xcolor', 'b', 'Ycolor', 'r', 'fontsize', 12);
622. grid on;
623. % *****Graph29*****
624. clear all;
625. DTmax=0:10:50;
626. CRa=119832.362;
627. E=0.9;
628. Qmax=CRa*DTmax;
629. Q=E*Qmax;
630. T2=34.7;
631. CR2=176156.059;
632. T3=((CR2*T2)-Q)/CR2;
633. txt=num2str(T3);
634. p3=94545;
635. pv3=[5.5432e+03 3.9171e+03 2.7228e+03 1.8597e+03 1.2465e+03
818.8925];
636. d3=0.62198*(pv3./(p3-pv3));
637. Mf2=162805.97;
638. d2=0.0383;
639. DMwater2=Mf2*((d2/(1+d2))-(d3./(1+d3)));

```

```

640. Mwg=0.9; g=9.81; H1=500;
641. pwg=Mwg*DMwater2*g*H1;
642. pat=39200000;
643. ptotal=pat+pwg;
644. figure();
645. plot(DTmax,ptotal,'*-r','linewidth',2);
646. str={'The maximum temperture differece at condenser inlets between', ...
647. 'operating air and ambient air \Delta\itT_{max} ({}^{\circ}C) '};

648. xlabel( str ,'fontsize',12,'fontweight','b','color','b');
649. ylabel('Power output \itW^{.}_{}_{total}
(W)', 'fontsize',12,'fontweight','b','color','r');
650. title('\Delta\itT_{max} & \itW^{.}_{}_{total}
','fontsize',13,'fontweight','b','color','k');
651. set(gca,'Xcolor','b','Ycolor','r','fontsize',12);
652. grid on;
653. % % % % % *****Graph30*****
654. clear all;
655. DTmax=0:10:50;
656. CRa=119832.362;
657. E=0.9;
658. Qmax=CRa*DTmax;
659. Q=E*Qmax;
660. T2=34.7;
661. CR2=176156.059;
662. T3=((CR2*T2)-Q)/CR2;
663. txt=num2str(T3);
664. p3=94545;
665. pv3=[5.5432e+03 3.9171e+03 2.7228e+03 1.8597e+03 1.2465e+03
818.8925];
666. d3=0.62198*(pv3./(p3-pv3));
667. Mf2=162805.97;
668. d2=0.0383;
669. DMwater2=Mf2*((d2/(1+d2))-(d3/(1+d3)));
670. Mwg=0.9; g=9.81; H1=500;
671. pwg=Mwg*DMwater2*g*H1;
672. pat=10300442980;
673. ptotal=pat+pwg;
674. Acoll=26786475.601;
675. s=1000;
676. Upp=ptotal./(Acoll*s);
677. Upp=Upp*100;
678. figure();
679. plot(DTmax,Upp,'*-r','linewidth',2);
680. str={'The maximum temperture differece at condenser inlets between', ...
681. 'operating air and ambient air \Delta\itT_{max} ({}^{\circ}C) '};

682. xlabel(str,'fontsize',12,'fontweight','b','color','b');
683. ylabel('Efficiency \eta\it_{\rho\rho}
(%)', 'fontsize',12,'fontweight','b','color','r');

```

```

684. title('\Delta\itT_{max} & \eta\it_{\rho\rho}
      ', 'fontsize', 13, 'fontweight', 'b', 'color', 'k');
685. set(gca, 'Xcolor', 'b', 'Ycolor', 'r', 'fontsize', 12);
686. grid on;
687. % % % % % % *****Graph31*****
688. pwg=14913196.335;
689. Eat=0:0.1:1;
690. pat=Eat*0.9*20106.192*7.58*357.23;
691. ptotal=pat+pwg;
692. figure();
693. plot(Eat, ptotal, '*-r', 'linewidth', 2);
694. xlabel('The Efficiency of air turbine generator
      (%)', 'fontsize', 12, 'fontweight', 'b', 'color', 'b');
695. ylabel('Power output \itW^{.}_{total}
      (W)', 'fontsize', 12, 'fontweight', 'b', 'color', 'r');
696. title('\eta\it_{at} & \itW^{.}_{total}
      ', 'fontsize', 13, 'fontweight', 'b', 'color', 'k');
697. set(gca, 'Xcolor', 'b', 'Ycolor', 'r', 'fontsize', 12);
698. grid on;
699. % % % % % % *****Graph32*****
700. format short;
701. pwg=10276156176.335;
702. Eat=0:0.1:1;
703. pat=Eat*0.9*20106.192*7.58*357.23;
704. ptotal=pat+pwg;
705. Acoll=26786475.601;
706. s=1000;
707. Upp=ptotal./(Acoll*s);
708. Upp=Upp*100;
709. figure();
710. plot(Eat, Upp, '*-r', 'linewidth', 2);
711. xlabel('The Efficiency of air turbine generator
      (%)', 'fontsize', 12, 'fontweight', 'b', 'color', 'b');
712. ylabel('Efficiency \eta\it_{\rho\rho}
      (%)', 'fontsize', 12, 'fontweight', 'b', 'color', 'r');
713. title('\eta\it_{at} & \eta\it_{\rho\rho}
      ', 'fontsize', 13, 'fontweight', 'b', 'color', 'k');
714. set(gca, 'Xcolor', 'b', 'Ycolor', 'r', 'fontsize', 12);
715. grid on;
716. % % % % % % *****Graph33*****
717. Ewg=0:0.1:1;
718. pwg=Ewg*3378.223*9.81*500;
719. pat=39200000;
720. ptotal=pat+pwg;
721. figure();
722. plot(Ewg, ptotal, '*-r', 'linewidth', 2);
723. xlabel('The Efficiency of water generator (%)
      ', 'fontsize', 12, 'fontweight', 'b', 'color', 'b');
724. ylabel('Power output \itW^{.}_{total}
      (W)', 'fontsize', 12, 'fontweight', 'b', 'color', 'r');

```

```

725. title('\eta\it_{wg} & \itW^{.}_{total}
      ', 'fontsize', 13, 'fontweight', 'b', 'color', 'k');
726. set(gca, 'Xcolor', 'b', 'Ycolor', 'r', 'fontsize', 12);
727. grid on;
728. % % % % % % *****Graph34*****
729. Ewg=0:0.1:1;
730. pwg=Ewg*3378.223*9.81*500;
731. pat=10300442980;
732. ptotal=pat+pwg;
733. Acoll=26786475.601;
734. s=1000;
735. Upp=ptotal./(Acoll*s);
736. Upp=Upp*100;
737. figure();
738. plot(Ewg,Upp, '*-r', 'linewidth', 2);
739. xlabel('The Efficiency of water generator
      (%)', 'fontsize', 12, 'fontweight', 'b', 'color', 'b');
740. ylabel('Efficiency \eta\it_{\rho\rho}
      (%)', 'fontsize', 12, 'fontweight', 'b', 'color', 'r');
741. title('\eta\it_{wg} & \eta\it_{\rho\rho}
      ', 'fontsize', 13, 'fontweight', 'b', 'color', 'k');
742. set(gca, 'Xcolor', 'b', 'Ycolor', 'r', 'fontsize', 12);
743. grid on;

```

Appendix 2: The code of MATLAB for economic model

```

1. clear all; clc;
2. % % *****Graph1*****
3. Rcoll=2000:500:4500;
4. Acoll=pi*((Rcoll-80).^2);
5. Upp=0.002;
6. s=1000;
7. ptotal=Upp*Acoll*s;
8. ptotal=ptotal./10^3; %Convert from W unit to KW unit
9. ptotal=ptotal./24;
10. noddy=365;
11. rhid=24;
12. Ppower=noddy*rhid*ptotal;
13. Poe=0.3;
14. Epower=Poe*Ppower;
15. figure();
16. plot(Rcoll,Epower,'*-r','linewidth',2);
17. xlabel('Collector radius \itR_{coll}
(m)','fontsize',12,'fontweight','b','color','b');
18. ylabel('annual revenue of electricity \itE_{power}
(EURO)','fontsize',12,'fontweight','b','color','r');
19. title('\itR_{coll} & \itE_{Power}','fontsize',13,'fontweight','b','color','k');
20. set(gca,'Xcolor','b','Ycolor','r','fontsize',12);
21. grid on;
22. % % *****Graph2*****
23. Dcoll=2*Rcoll;
24. Fpp=(pi/4)*((Dcoll.^2) -
(2*80)^2)*9+pi*2*80*500*250+0.5e6+(pi/4)*((2*80)^2)*18;
25. Fyr=Fpp*0.0797;
26. Cost_water=(Fyr-401541.3182-Epower)/(143185202.928/(1000*1e-3));
27. figure();
28. plot(Rcoll,Cost_water,'*-r','linewidth',2);
29. xlabel('Collector radius \itR_{coll}
(m)','fontsize',12,'fontweight','b','color','b');
30. ylabel('Price of fresh water \itcost_{water} (EURO \it.m^{-}
3)'),'fontsize',12,'fontweight','b','color','r');
31. title('\itR_{coll} & \itcost_{water}','fontsize',13,'fontweight','b','color','k');
32. set(gca,'Xcolor','b','Ycolor','r','fontsize',12);
33. grid on;
34. % % % % *****Graph3*****
35. clear all;
36. clc;
37. H1=300:200:1300;
38. Pwg=0.9*3378.223*9.81*H1;
39. Ptotal=39200000+Pwg;

```

```

40. Ptotal=(Ptotal/24)/1000; %Convert from wh to Kwh
41. noddy=365;
42. rhid=24;
43. Ppower=noddy*rhid*Ptotal;
44. Poe=0.3;
45. Epower=Poe*Ppower;
46. figure();
47. plot(H1,Epower,'*-r','linewidth',2);
48. xlabel('Chimney height \itH_1 (m)','fontsize',12,'fontweight','b','color','b');
49. ylabel('annual revenue of electricity \itE_{W annual}
(EURO)','fontsize',12,'fontweight','b','color','r');
50. title('\itH_1 & \itE_{Power}','fontsize',13,'fontweight','b','color','k');
51. set(gca,'Xcolor','b','Ycolor','r','fontsize',12);
52. grid on;
53. % % % % *****Graph4*****
54. Fpp=(pi/4)*((6000.^2) -
160^2)*9+pi*160*H1*250+0.5e6+(pi/4)*(160^2)*18;
55. Fyr=Fpp*0.0797;
56. Cost_water=(Fyr-401541.3182-5925351.6)/(143185202.928/(1000*1e-3));
57. figure();
58. plot(H1,Cost_water,'*-r','linewidth',2);
59. xlabel('chimney height \itH_1 (m)','fontsize',12,'fontweight','b','color','b');
60. ylabel('Price of fresh water \itcost_{water} (EURO \it.m^{-
3}),'fontsize',12,'fontweight','b','color','r');
61. title('\itH_1 & \itcost_{water}','fontsize',13,'fontweight','b','color','k');
62. set(gca,'Xcolor','b','Ycolor','r','fontsize',12);
63. grid on;
64. % % % % *****Graph5*****
65. clc;
66. clear all;
67. n=[5 ,15, 25,30,35,40];
68. for k= 1:6
69. z(k)=(0.062*(1+0.062)^n(k))/(((1+0.062)^n(k))-1);
70. Fyr(k)=317852717.0717*z(k);
71. end
72. figure();
73. plot(n,Fyr,'*-r','linewidth',2);
74. xlabel('service life of integrated system n (years)
','fontsize',12,'fontweight','b','color','b');
75. ylabel('annual average investiment \itF_{yr}
(EURO)','fontsize',12,'fontweight','b','color','r');
76. title('n & \itF_{yr}','fontsize',13,'fontweight','b','color','k');
77. set(gca,'Xcolor','b','Ycolor','r','fontsize',12);
78. grid on;
79. % % % % *****Graph6*****
80. Cost_water=(Fyr-401541.3182-5925351.6)/(143185202.928/(1000*1e-3));
81. figure();
82. plot(n,Cost_water,'*-r','linewidth',2);
83. xlabel('service life of integrated system n
(years)','fontsize',12,'fontweight','b','color','b');

```

```

84. ylabel('Price of fresh water \itcost_{water} (EURO \it.m^{\{-
    3})), 'fontsize',12,'fontweight','b','color','r');
85. title('n & \itcost_{water}', 'fontsize',13,'fontweight','b','color','k');
86. set(gca,'Xcolor','b','Ycolor','r','fontsize',12);
87. grid on;
88. % % % *****Graph7*****
89. clc;
90. clear all;
91. i=[0.05:0.01:0.1];
92. ii=5:10;
93. for k=1:6;
94. z(k)=(i(k)*(1+i(k))^25)/(((1+i(k))^25)-1);
95. end
96. Fyr=317852717.0717*z;
97. figure();
98. plot(ii,Fyr,'*-r','linewidth',2);
99. xlabel('annual interest rate i (%)','fontsize',12,'fontweight','b','color','b');
100. ylabel('annual average investment \itF_{yr}
    (EURO)', 'fontsize',12,'fontweight','b','color','r');
101. title('i & \itF_{yr}', 'fontsize',13,'fontweight','b','color','k');
102. set(gca,'Xcolor','b','Ycolor','r','fontsize',12);
103. grid on;
104. % % % % *****Graph8*****
105. Cost_water=(Fyr-401541.3182-5925351.6)/(143185202.928/(1000*1e-
    3));
106. figure();
107. plot(ii,Cost_water,'*-r','linewidth',2);
108. xlabel('annual interest rate i (%)','fontsize',12,'fontweight','b','color','b');
109. ylabel('Price of fresh water \itcost_{water} (EURO \it.m^{\{-
    3})), 'fontsize',12,'fontweight','b','color','r');
110. title('i & \itcost_{water}', 'fontsize',13,'fontweight','b','color','k');
111. set(gca,'Xcolor','b','Ycolor','r','fontsize',12);
112. grid on;
113. % % % % *****Graph9*****
114. clc;
115. clear all;
116. Nu=[5 6 7 8 9 24];
117. Ptotal=2254.7
118. noddy=365;
119. Ppower=noddy*Nu*Ptotal;
120. figure();
121. plot(Nu,Ppower,'*-r','linewidth',2);
122. xlabel('Runnig hours of integrated system in a day
    Nu/hours','fontsize',11,'fontweight','b','color','b');
123. ylabel('annual power output \itP_{power} /
    kwh', 'fontsize',11,'fontweight','b','color','r');
124. title('Nu & \itP_{power}', 'fontsize',13,'fontweight','b','color','k');
125. set(gca,'Xcolor','b','Ycolor','r','fontsize',12);
126. grid on;
127. % % % % *****Graph10*****

```



```

128. Poe=0.3;
129. Epower=Poe*Ppower;
130. figure();
131. plot(Nu,Epower,'*-r','linewidth',2);
132. xlabel('Runnig hours of integrated system in a day
        Nu/hours','fontsize',11,'fontweight','b','color','b');
133. ylabel('annual revenue electricity \itE_{power} /
        EURO','fontsize',11,'fontweight','b','color','r');
134. title('Nu & \itE_{Power}','fontsize',13,'fontweight','b','color','k');
135. set(gca,'Xcolor','b','Ycolor','r','fontsize',12);
136. grid on;
137. % % % *****Graph11*****
138. Mco2=0.95*Ppower;
139. figure();
140. plot(Nu,Mco2,'*-r','linewidth',2);
141. xlabel('Runnig hours of integrated system in a day
        Nu/hours','fontsize',11,'fontweight','b','color','b');
142. ylabel('amount of \itCo_2 emission reduction \itMco_2 /
        ton','fontsize',11,'fontweight','b','color','r');
143. title('Nu & \itMco_2','fontsize',13,'fontweight','b','color','k');
144. set(gca,'Xcolor','b','Ycolor','r','fontsize',12);
145. grid on;
146. % % % *****Graph12*****
147. Eco2=21.4*Mco2;
148. figure();
149. plot(Nu,Eco2,'*-r','linewidth',2);
150. xlabel('Runnig hour of integrated system in a day
        Nu/hours','fontsize',11,'fontweight','b','color','b');
151. ylabel('annual revenue of carbon credits \itEco_2 /
        EURO','fontsize',11,'fontweight','b','color','r');
152. title('Nu & \itEco_2','fontsize',13,'fontweight','b','color','k');
153. set(gca,'Xcolor','b','Ycolor','r','fontsize',12);
154. grid on;
155. % % % *****Graph13*****
156. Mwater=365*Nu*3600*(1162.15+3378.223)*10^-3;
157. figure();
158. plot(Nu,Mwater,'*-r','linewidth',2);
159. str={'annual fresh water productivity of integrated system', ...
160.     ' '};
161. \itM_{Water} / ton '
162. xlabel('Runnig hours of integrated system in a day
        Nu/hours','fontsize',11,'fontweight','b','color','b');
163. ylabel( str ,'fontsize',11,'fontweight','b','color','r');
164. title('Nu & \itM_{water}','fontsize',13,'fontweight','b','color','k');
165. set(gca,'Xcolor','b','Ycolor','r','fontsize',12);
166. grid on;
167. % % % *****Graph14*****
168. Cost_water=(25332861.55-401541.3182-
        5925351.6)./(Mwater/(1000/1000));
169. figure();

```

```

170. plot(Nu, Cost_water, '*-r', 'linewidth', 2);
171. xlabel('Runnig hours of integrated system in a day
Nu/hours', 'fontsize', 11, 'fontweight', 'b', 'color', 'b');
172. ylabel('Price of fresh water \itcost_{water}/ EURO \itm^{-3}', 'fontsize', 11, 'fontweight', 'b', 'color', 'r');
173. title('Nu & \itCost_{water}', 'fontsize', 13, 'fontweight', 'b', 'color', 'k');
174. set(gca, 'Xcolor', 'b', 'Ycolor', 'r', 'fontsize', 12);
175. grid on;
176. % % % *****Graph15*****
177. clc;
178. clear all;
179. DMwater1and2=1000:1000:6000;
180. Mwater=365*24*3600*(DMwater1and2)*10^-3;
181. Cost_water=(25332861.55-401541.3182-5925351.6)./(Mwater/(1000*10^-3));
182. str={'Mass Flow rate of condensed vapor in the chimney and in the
condenser', ...
183. ' ', ...
184. '(\itm^{.}_{water1} + \itm^{.}_{water2}) (kg \it.s^{-1}) '};
185. figure();
186. plot(DMwater1and2, Cost_water, '*-r', 'linewidth', 2);
187. xlabel(str, 'fontsize', 12, 'fontweight', 'b', 'color', 'b');
188. ylabel('Price of fresh water \itcost_{water} (EURO \it.m^{-3})', 'fontsize', 12, 'fontweight', 'b', 'color', 'r');
189. title('(\itm^{.}_{water1} + \itm^{.}_{water2}) & \itCost_{water}', 'fontsize', 13, 'fontweight', 'b', 'color', 'k');
190. set(gca, 'Xcolor', 'b', 'Ycolor', 'r', 'fontsize', 12);
191. grid on;

```